

11-12-1995  
118-1R  
007242

**Minimum Heating Re-Entry Trajectories for  
Advanced Hypersonic Launch Vehicles**

By

Robert Windhorst

**THESIS**

Submitted in Partial Fulfillment of the Requirements for the  
Masters Degree in  
Mechanical Engineering in the School of Engineering  
Santa Clara University, 1996

Santa Clara, California

## ACKNOWLEDGMENT

Special thanks is given to my advisor Dr. Mark Ardema for providing the guidance and knowledge necessary for putting together this thesis and to Jeff Bowles for his exciting ideas which brought about this research.

I also thank my parents for their continual love and support.

This research was supported by NASA Ames Research Center Grant NCC2-5165.

## TABLE OF CONTENTS

	Page
1 Introduction	1
2 Methods	2
2.1 Vehicle Synthesis Code	2
2.2 Constraints	3
2.3 Energy State Approximation	3
2.4 Temperature Estimation	4
2.5 Heat Transfer Analysis	5
3 Results	8
3.1 Minimum Q Trajectories	8
3.2 Maximum Q Trajectories	10
3.3 Integral $T_{\text{surf}}$ dt Trajectory	12
4 Conclusions	13
References	14
Tables and Figures	

# **Minimum Heating Re-Entry Trajectories for Advanced Hypersonic Launch Vehicles**

Robert Windhorst

Department of Mechanical Engineering  
Santa Clara University  
Santa Clara, California

## **Abstract**

Optimal re-entry trajectories are generated for reusable launch vehicles which minimize: (i) the heat absorbed at the vehicle surface, (ii) the lower surface temperature, and (iii) the heat absorbed by the internal structure. The approach uses the energy state approximation technique and a finite control volume heat transfer code coupled to a flight path integration code. These trajectories are compared to the optimal re-entry trajectory minimizing the integrated convective heat rate to determine which trajectory produces the minimum internal structural temperatures for a given thermal protection system. Three different thermal protection systems are considered: tile, blanket, and metallic.

## Nomenclature

$c$	=	specific heat, btu/(lb*R)
$dt$	=	time step required by vehicle to travel between energy levels, sec
$\epsilon$	=	emissivity
$k$	=	thermal conductivity, btu/(hr*ft*R)
$L$	=	total thickness of TPS
$P$	=	vehicle specific excess power, ft/sec
$P_{surf}$	=	pressure at vehicle surface, lb/ft <sup>2</sup>
$\Phi$	=	optimization function
$\Phi$	=	integrated optimization function
$q$	=	dynamic pressure, lb/ft <sup>2</sup>
$\dot{Q}_{abs}$	=	conductive heat rate per square foot, btu/(hr*ft <sup>2</sup> )
$Q_{abs}$	=	total heat conducted per square foot, btu/ft <sup>2</sup>
$\dot{Q}_{conv}$	=	convective heat rate per square foot, btu/(hr*ft <sup>2</sup> )
$Q_{conv}$	=	total heat convected per square foot, btu/ft <sup>2</sup>
$\dot{Q}_{rad}$	=	radiative heat rate per square foot, btu/(hr*ft <sup>2</sup> )
$Q_{rad}$	=	total heat radiated per square foot, btu/ft <sup>2</sup>
$\rho$	=	density, lb/ft <sup>3</sup>
$\sigma$	=	Stephan-Boltzmann cons., btu/(hr*ft <sup>2</sup> *R <sup>4</sup> )
$t$	=	flight time, min.
$T_{surf}$	=	temperature @ vehicle surface, °F
$T_i$	=	temperature of TPS node i, °F
$x$	=	TPS depth measured from surface, inches

## 1. Introduction

Current research and development of advanced reusable launch vehicles (RLVs) focuses on reducing the cost of access to space and the turn around time between missions. The RLV program proposes to reduce operating cost and turn around in part by redesigning the vehicle thermal protection system (TPS) for lighter weight, reusability, and increased durability relative to the space shuttle. There are two key interrelated aspects of launch vehicle TPS design: optimizing the vehicle re-entry trajectory for minimum internal structural temperatures for a given TPS, and evaluation of advanced, lightweight, reusable TPS materials. Although this report concentrates on the trajectory optimization problem, results are given for three different TPS concepts: tile, blanket, and metallic. The tile and blanket TPS concepts are similar to what is currently used on the space shuttle. The underside of the shuttle uses a tile TPS and the top side uses a blanket TPS. The metallic TPS, however, represents a new TPS concept designed for the goals mentioned above: lighter weight, reusability, and increased durability.

As a RLV descends into the atmosphere from orbit it undergoes extreme convective heat rates ( $\dot{Q}_{\text{conv}}$ ) due to its high kinetic energy. The magnitude and duration of  $\dot{Q}_{\text{conv}}$  determine the thickness of the TPS required to prevent the vehicle internal structure temperature from exceeding its limit. In Reference 1 this problem is approached by using the energy state trajectory approximation [Ref. 2-5] to minimize the required thickness of the TPS by minimizing the integrated convective heat rate ( $Q_{\text{conv}}$ ) on the vehicle.

Sachs and Dinkelmann [Ref. 6] minimize fuel consumption of a hypersonic vehicle subject to a heat absorption constraint ( $Q_{\text{limit}}$ ). The vehicle is an air-breathing first stage of a two-stage launch system. Because the maximum speed is Mach 6, kinetic energies and  $\dot{Q}_{\text{conv}}$  are much lower than for the re-entry of single stage vehicles. The constraint on the heat absorbed by the vehicle used in Ref. 6 is

$$\int_0^{t_f} \dot{Q}_{abs} dt \leq Q_{limit}$$

where  $\dot{Q}_{abs}$  is the rate of heat absorbed by the innermost layer of the insulation and is determined by a finite difference heat transfer code much like the one used in the present paper. Since  $Q_{limit}$  is evaluated at the end of the mission, Sachs and Dinkelmann must solve a two point boundary value trajectory optimization problem. They found that the heat absorbed could be greatly reduced with only a small penalty in fuel consumption.

The approach used in this paper avoids the complexity of the two point boundary value problem by using the energy state approximation (ESA) technique [Ref. 2-5]. By the ESA technique optimal trajectories minimizing a variety of different functions can be generated with a single integration of the equations of motion over the vehicle flight path. Furthermore, ESA techniques could be used to write an on-board algorithm that uses position feedback to generate optimal trajectories in real time [Ref. 5]. This paper presents results of optimal trajectories minimizing: (i) the heat absorbed ( $Q_{abs}$ ) by the RLV at its surface, (ii) the RLV estimated lower surface temperature, and (iii) the heat absorbed by the RLV internal structure, and compares them to results obtained by minimizing  $Q_{conv}$ , as is done in Reference 1, to determine which trajectory minimizes the internal structural temperatures of the RLV for a given thermal protection system. Also discussed are the assumed vehicle constraints on the flight trajectory, the method of generating approximate optimal trajectories, and the equations for calculating temperatures and conductive heat rates ( $\dot{Q}_{abs}$ ).

## 2. Methods

### 2.1 Vehicle Synthesis Code

The NASA AMES Hypersonic Advanced Vehicle Optimization Code (HAVOC) generated all the optimal trajectories presented in this

paper. HAVOC aides RLV design by synthesizing key vehicle elements such as geometry, aerodynamics, dynamics, propulsion, and structures into a single code. The integration of all these elements into a single code creates a versatile platform ideal for studying RLV optimal trajectories. Furthermore, the code contains built in subroutines which use energy state approximation (ESA) techniques to generate optimal trajectories minimizing time, fuel,  $Q_{conv}$ ,  $Q_{abs}$ , or a weighted combination of these [Ref. 1]. Although the optimal paths are determined from ESA methods, the trajectory integration in HAVOC uses a point mass model assuming a spherical rotating earth with no winds and a flight path angle rate of zero. The equations of motion are listed as equation (1) in Reference 2.

## 2.2 Constraints

There are seven vehicle constraints imposed on the flight trajectories. Each constraint along with its upper and/or lower limit is listed in Table 1. The first constraint is imposed on the dynamic pressure ( $q$ ) of the vehicle. Three temperature constraints are imposed at three different locations on the vehicle body. TSTAGN is the stagnation temperature constraint at the vehicle nose.

Temperature lower surface (TLS) is the temperature constraint of a point located along the windward surface, centerline, and 1/3 the vehicle length from the nose, and temperature upper surface (TUS) is the temperature constraint of a point located along the leeward surface, centerline, and 1/3 the vehicle length from the nose. The load factor (SLDFAC) constraint limits the acceleration of the vehicle in the direction normal to the velocity vector. AN is the constraint on the vehicle's angle of attack, and FA is the constraint on the vehicle's flight path angle.

## 2.3 Energy State Approximation

The ESA method of trajectory optimization generates an optimal trajectory minimizing the integral

$$\Phi = \int \dot{\Phi} \frac{dE}{P} \quad (1)$$



where  $\dot{\Phi}$ , called the optimization function, is the vehicle parameter of interest,  $P$  is the specific excess power of the vehicle, and  $dE$  is the energy step [Ref. 2-5]. This approach assumes that the energy state variable is on a slower time scale than the other trajectory and temperature variables. Substituting

$$\frac{dE}{P} = dt \quad (2)$$

into equation (1) results in

$$\Phi = \int \dot{\Phi} dt \quad (3)$$

Therefore by equation (3) the optimal trajectory generated using the ESA technique directly minimizes the integral of  $\dot{\Phi}$  with respect to time. We note that  $E$  is preferable to  $t$  as an independent variable because its total change is the same for every trajectory.

## 2.4 Temperature Estimation

In addition to its optimal trajectory and vehicle dynamics routines, HAVOC contains a subroutine TEMP which estimates vehicle surface temperature ( $T_{surf}$ ). HAVOC uses engineering approximations in its aerothermal subroutines to construct for each surface panel on the RLV  $\dot{Q}_{conv}$  as a numerical function of  $\alpha$ , altitude, and Mach number. HAVOC then calculates  $T_{surf}$  for a given surface panel using the following energy balance equation:

$$\dot{Q}_{conv} = \dot{Q}_{rad} \quad (4)$$

$$\dot{Q}_{conv} = \epsilon \sigma [T_{surf}^4 - T_{amb}^4] \quad (5)$$

$$T_{surf} = \left[ \frac{\dot{Q}_{conv}}{\epsilon \sigma} + T_{amb}^4 \right]^{\frac{1}{4}} \quad (6)$$

The absence of conduction terms in the surface energy balance equation slightly inflates  $T_{surf}$  and does not calculate the conductive heat rates ( $\dot{Q}_{abs}$ ) of the TPS.

## 2.5 Heat Transfer Analysis

The HAVOC subroutine HEATX receives inputs of time step, surface pressure,  $\dot{Q}_{conv}$ , and past nodal temperatures. HEATX outputs  $\dot{Q}_{abs}$  and current TPS nodal temperatures (see Table 2). HAVOC integrates  $\dot{Q}_{abs}$  with respect to time to find the total heat absorbed ( $Q_{abs}$ ). Both the TEMP and HEATX calculations are made at a single point on the vehicle body. For this study this point is at the same location as the TLS temperature constraint, along the windward surface, centerline, and 1/3 the vehicle length from the nose.

HEATX solves the one dimensional transient heat equation,

$$\rho c \frac{\partial T}{\partial t} - \frac{\partial}{\partial x} \left[ k \frac{\partial T}{\partial x} \right] = 0 \quad (7)$$

where

$$T=f(x,t) \quad 0 \leq x \leq L \quad (8)$$

$$c=f(T) \quad 255 \text{ min} \leq t < \infty \quad (9)$$

$$k=f(T, P_{surf}) \quad (10)$$

where  $L$  is the thickness of the TPS and the RLV re-enters the atmosphere 255 minutes into its mission. Equation (7) is a linear partial differential equation with the initial condition

$$T(x, 255) = 70^\circ\text{F} \quad (11)$$

and boundary conditions

$$@x=0 \quad -k \frac{\partial T}{\partial x} = \dot{Q}_{conv} - \epsilon \sigma [T^4 - T_{amb}^4] \quad (12)$$

$$\text{@}x=L \quad -k \frac{\partial T}{\partial x} = 0 \quad (13)$$

The 70°F initial temperature arises from what is currently done with the space shuttle. Just before the shuttle leaves orbit to make its descent, it performs a series of 360° rolls in the sun. These rolls are intended to create an even temperature distribution around the shuttle TPS at approximately 70°F. The TPS surface boundary condition at  $x=0$  imposes the law of conservation of energy, forcing the sum of  $\dot{Q}_{\text{conv}}$ ,  $\dot{Q}_{\text{rad}}$ , and  $\dot{Q}_{\text{abs}}$  at the surface to zero. The tank TPS boundary condition at  $x=L$  is adiabatic. The adiabatic boundary condition arises from the assumption of a dry tank wall. This assumption is justified by the fact the vehicle has used up all its fuel during ascent. Since the fuel tank is empty, any heat reaching the tank has no where to go and therefore can only be used in heating the tank structure.

HEATX generates the solution to equation (7) using numerical techniques. A 1-D section of the TPS is divided up into  $n$  number of nodes. Figure 1 illustrates the nodal breakdown of the TPS section and the five different types of nodes: inner layer nodes, TPS surface boundary nodes, TPS tank boundary nodes, layer boundary nodes, and layer boundary nodes with an air or vacuum gap. Table 3 lists for each TPS the number of layers, layer thickness, layer material, layer weight, and number of nodes in each layer. Equation (7) is discretized using the control volume formulation, resulting in a set of  $n$  equations, one for each node, and  $n$  unknowns, the temperature of each node [Ref. 7]. The generalized equation for each type of node is as follows:

#### 1) Inner Layer Node

$$\frac{k_e}{\Delta x} [T_{i+1} - T_i] - \frac{k_e}{\Delta x} [T_i - T_{i-1}] = \frac{\rho c}{\Delta t} [T_i - T_{i,\text{past}}] \quad (14)$$

#### 2) TPS Surface Boundary Node @ $x=0$

$$-\frac{k_e}{\Delta x}[T_2 - T_1] = \dot{Q}_{conv} - \epsilon \sigma [T_1^4 - T_{amb}^4] \quad (15)$$

3) TPS Tank Boundary Node @  $x=L$

$$T_n - T_{n-1} = 0 \quad (16)$$

4) Layer Boundary Node

$$\frac{k_e}{\Delta x}[T_{i+1} - T_i] - \frac{k_e}{\Delta x}[T_i - T_{i-1}] = 0 \quad (17)$$

5) Layer Boundary Node with a gap

equation for gap upper surface node  $T_i$

$$-\frac{k_e}{\Delta x}[T_i - T_{i-1}] = \epsilon_e \sigma [T_i^4 - T_{i+1}^4] + h_\infty [T_i - T_{i+1}] \quad (18)$$

equation for gap lower surface node  $T_{i+1}$

$$-\frac{k_e}{\Delta x}[T_{i+2} - T_{i+1}] = \epsilon_e \sigma [T_i^4 - T_{i+1}^4] + h_\infty [T_i - T_{i+1}] \quad (19)$$

These equations are linearized, grouped into a matrix, and solved for the nodal temperatures. Once the nodal temperatures are known,  $\dot{Q}_{abs}$  may be calculated by (20). Equation (21) calculates  $\dot{Q}_{abs}$  at the vehicle surface, while equation (22) calculates  $\dot{Q}_{abs}$  at the vehicle structure. The subscript  $m$  in equation (22) denotes the layer boundary node between the aluminum structure layer and the layer just before it.

$$\dot{Q}_{abs} = -k \frac{\partial T}{\partial x} \quad (20)$$

$$\dot{Q}_{abs, surf} = -\frac{k}{\Delta x}[T_2 - T_1] \quad (21)$$

$$\dot{Q}_{abs, tank} = -\frac{k}{\Delta x}[T_{m+1} - T_m] \quad (22)$$

### 3. Results

Table 4 lists the four different optimization functions compared in this report, and figure 2 illustrates the optimal trajectory HAVOC generated for each optimization function. Also plotted on figure 2 is the space shuttle trajectory taken from reference 6. The space shuttle trajectory agrees well with the case 2 optimal trajectory. In addition to the optimization functions, table 4 gives the vehicle descent time and maximum structural temperature for each case. The four optimal trajectories are grouped into the following two categories: minimum  $q$  trajectories and maximum  $q$  trajectories. Cases 1-3 are minimum  $q$  trajectories, while case 4 is a maximum  $q$  trajectory.

#### 3.1 Minimum $q$ Trajectories

Minimum  $q$  trajectories follow the minimum  $q$  boundary of the flight envelope and are typically constrained by either max. AN or min.  $q$ . As shown in figure 2, the case 1-3 trajectories conserve potential energy, while bleeding off kinetic energy. These lofted trajectories maintain low  $\dot{Q}_{conv}$ , producing relatively low  $\dot{Q}_{abs}$  and surface temperatures. Figure 3 illustrates the low  $\dot{Q}_{conv}$ , figures 4.1-4.3 illustrate the low  $\dot{Q}_{abs}$ , and figures 5.1-5.3 illustrate the low surface temperatures for the three TPSs. These trajectories induce relatively low drag on the vehicle, resulting in relatively large descent times. The case 1-3 descent times in table 4 are all larger than the case 4 descent time. Therefore, optimization functions which produce minimum  $q$  trajectories emphasize minimum  $\dot{Q}_{conv}$  at the expense of descent time.

##### Case #1

HAVOC generated the case 1 optimal trajectory using  $\dot{Q}_{abs}$  at the vehicle surface, equation (21), as the optimization function. By the ESA, the case 1 optimal trajectory should minimize  $\dot{Q}_{abs} \cdot dt$  per specific energy change of the vehicle. Figures 6.1-6.3 show that this

is always true. At a specific energies between 2500 ft and 4500 ft the case 1 curve is not the lowest curve on the plots. The cause for this discrepancy is that the heat equation dynamics are directly coupled into the vehicle flight dynamics. In principle, the coupling of the heat dynamics with the flight dynamics violates the ESA assumption that energy is the only state variable of the system. Although this assumption is violated, the case 1 optimal trajectory still results in the lowest  $Q_{abs}$  at landing, see figures 7.1-7.3, implying the coupling between the heat dynamics and flight dynamics is weak and may be neglected.

As shown in figures 7.1-7.3, after the vehicle has landed, heat continues to radiate off of the vehicle surface thus decreasing  $Q_{abs}$  of the vehicle. Because of transient effects, the vehicle structure reaches its maximum temperature well after the vehicle has landed, see figures 8.1-8.3. This transient effect is further illustrated by figure 9. Notice in figure 9 that after the maximum surface temperature has been reached a heat pulse travels from the TPS surface to the vehicle structure. This heat pulse continues to increase the temperature of the vehicle structure even after surface temperatures have started to cool. Table 4 shows that the case 1 optimal trajectory results in the longest descent time and the highest maximum structural temperature of the vehicle.

## Case # 2

HAVOC generated the case 2 optimal trajectory using  $T_{surf}^4$  as the optimization function. The TEMP subroutine calculates  $T_{surf}$ , and inspection of equation (5) reveals  $T_{surf}^4$  is directly proportional to  $\dot{Q}_{conv}$ . Figure 10 shows that the case 2 optimal trajectory minimizes  $\dot{Q}_{conv} \cdot dt$  per specific energy change of the vehicle, and figure 11 shows this optimal trajectory results in the lowest  $Q_{conv}$ .

The case 2 optimal trajectory follows a lofted path similar to the case 1 optimal trajectory. The  $T_{surf}^4$  term in the optimization function out weighs the  $dt$  term in the optimization integral forcing the trajectory into in the part of the flight envelop with relatively low  $\dot{Q}_{conv}$ . Again

because the case 2 optimal trajectory is lofted it results in a long descent time. The case 2 optimal trajectory results in the lowest maximum structural temperature of the vehicle, see figures 8.1-8.3.

### Case #3

For case 3 HAVOC did not use the ESA technique, rather it choose only the points within the flight envelope with the lowest  $T_{surf}$  for its optimal trajectory. Figure 12 shows the case 3 trajectory has the lowest  $T_{surf}$  per specific energy change the vehicle undergoes. The case 3 optimal trajectory was created independent of  $dt$ . It is very similar to the case 1 and case 2 optimal trajectories, further supporting the theory that the optimization functions which generate minimum  $q$  trajectories emphasize minimum  $T_{surf}$  and  $\dot{Q}_{conv}$  at the expense of time.

## 3.2 Maximum $q$ Trajectories

Maximum  $q$  trajectories attempt to follow the maximum  $q$  boundary of the flight envelope. As shown in figure 2 the case 4 trajectory exchanges potential energy for kinetic energy right away. It quickly dives deep into the atmosphere producing high  $\dot{Q}_{conv}$ , see figure 3, and drag. The high  $\dot{Q}_{conv}$  drives  $T_{surf}$  extremely high, so high that the trajectory must be constrained for the first half of the vehicle descent by TSTAGN. The high drag produced by these trajectories dissipates the vehicle's kinetic energy quickly, resulting in short vehicle descent times. Therefore maximum  $q$  trajectories produce relatively high  $\dot{Q}_{abs}$ , see figures 4.1-4.3, and surface temperatures, see figures 5.1-5.3, for short periods of time. Optimization functions which produce these trajectories emphasize minimizing  $dt$  at the expense of increasing the  $\dot{Q}_{conv}$ .

### Case #4

HAVOC generated the case 4 optimal trajectory using  $\dot{Q}_{abs}$  at the vehicle structure, equation (22), as the optimization function. Case 4 has the same problem as case 1 of coupling the heat dynamics with the vehicle dynamics. Again the coupling is assumed to be weak

and negligible. Figures 13.1-13.3 agree with this assumption and shows the case 4 optimal trajectory indeed minimizes  $\dot{Q}_{abs} \cdot dt$  per specific energy change of the vehicle.

The case 4 optimal trajectory is identical to the minimum time trajectory generated by an optimization function of 1. Figure 14 illustrates the case 4 optimal trajectory minimizing  $dt$  per specific energy change of the vehicle. According to table 4 the case 4 optimal trajectory has the lowest vehicle descent time.

The case 4 trajectory lies on the maximum nose cap stagnation temperature boundary for the first portion of the descent. If this condition is relaxed from 3000°F to 4000°F, a significant improvement results. Case 4 and this case, labeled 4\*, are compared on Figure 15. Case 4\* gives a trajectory which rapidly dives to the high  $q$  region (the load factor constraint was ignored for this dive) and stays there for the duration of the descent. Table 4 and Figure 16 show that this trajectory not only has minimum time but the lowest internal structural temperature as well.

The superiority of case 4\* is due to two factors: first, the amount of time the vehicle undergoes convective heating determines how far the heat will diffuse into the TPS. A short descent time and a TPS with low thermal diffusivity does not allow the heat to diffuse into the TPS very far. Constraining the heat near the surface of the TPS makes a shorter path for the heat to radiate back out of the vehicle instead of continuing to conduct further into the vehicle structure. Second the high  $T_{surf}$  caused by a case 4\* optimal trajectory increases the heat rejection rate,  $\dot{Q}_{rad}$ , by  $T_{surf}$  to the fourth power, see equation (5). Thus, although the case 4\* trajectory induces higher heat absorption rates on the vehicle, it allows even higher heat rejection rates. The combined effect of the short descent time and increased efficiency of heat rejection, keeps the heat at the TPS surface, rejects the heat quickly, and reduces conduction into the vehicle structure, thereby minimizing the maximum structural temperature of the vehicle. These combined effects are illustrated



in figure 17, which shows TPS temperature profiles for each case at the time when peak surface temperatures occurred. Notice the case 4\* profile has the highest surface temperature and the least amount of heat diffusion.

Chattering trajectories were also considered. In these trajectories, the vehicle rapidly banks left and right so that its flight path remains straight. This increases the vehicle lift and hence its drag.

Although chattering drastically reduces descent time by increasing drag, it also increases  $\dot{Q}_{conv}$ , thereby increasing  $T_{surf}$ . Since the vehicle is constrained by TSTAGN already during the first half of its descent, chattering does not significantly change the case 4 optimal trajectory unless the TSTAGN constraint is relaxed.

### 3.3 Integral $T_{surf}$ dt Trajectory

Trajectories were also generated minimizing the integral of  $T_{surf}$  with respect to time. This optimization integral is proportional to the integral of the steady state conductive heat rate of the vehicle, assuming the vehicle tank wall temperature remains constant.

$$\dot{Q}_{steady} = \frac{k_c}{L} [T_{surf} - T_{tank, wall}] \quad (23)$$

The integral  $T_{surf}$  dt optimal trajectory continually jumps between high q trajectories and low q trajectories. This is because  $T_{surf}$  and dt are now weighted equally, and low q trajectories minimize  $T_{surf}$  and high q trajectories minimize dt. Although jumping from one path to another is physically impossible, it is allowable by the ESA method. Constraining the trajectory with load factor limits eliminates the jumps but destroys the optimality of the trajectory. For example, a constrained integral  $T_{surf}$  dt trajectory that starts out as a low q trajectory is forced to remain a low q trajectory because of the load factor constraint. On the other hand, the integral  $T_{surf}$  dt trajectory could be forced to follow the high q trajectory at first and it would remain on that trajectory due to the load factor constraint.

#### 4. Concluding Remarks

Control volume heat transfer equations have been coupled to the re-entry flight dynamics equations for the purpose of determining trajectories that minimize heat input and interior structural temperatures. The energy state approximation was used to obtain the near-optimal paths.

It was found that the trajectories were of two types: very low dynamic pressure ( $q$ ) and very high  $q$ . The low  $q$  trajectories have lower surface temperatures and higher descent times than do the high  $q$  ones. The low  $q$  trajectories gave lower structural temperatures, but the difference was very small. If TPS materials capable of higher temperatures could be developed, then the high  $q$  trajectories become superior.

Finally, we note that the technique developed in this paper is non-iterative and has modest computational requirements. Thus it could be used as an on board guidance scheme to generate minimum heating trajectories in real time.

## References

- [1] H.C. Chow, M.D. Ardema, and J.V. Bowles, "Near Optimal Re-entry Trajectories for Reusable Launch Vehicles," to be submitted.
- [2] M. D. Ardema, J V. Bowles, and T. Whittaker, "Optimal Trajectories for Hypersonic Launch Vehicles," Dynamics and Control, Vol. 4, pages 337-347 (1994).
- [3] M. D. Ardema, J V. Bowles, E. J. Terjesen, and T. Whittaker, "Approximate Altitude Transitions for High-Speed Aircraft," Journal of Guidance, Control, and Dynamics, Vol. 18, No. 3, pages 561-566.
- [4] M.D. Ardema, J.V. Bowles, T. Whittaker, "Near-Optimal Propulsion-System Operation for an Air-Breathing Launch Vehicle," Journal of Spacecraft and Rockets, Vol. 32, No. 6, pages 951-956.
- [5] M.D. Ardema, H. C. Chow, and J.V. Bowles, "Near-Optimal Operation of Dual Fuel Vehicles," Journal of Guidance, Control, and Dynamics, Vol. 19, No. 5, pages 1180-1182.
- [6] G. Sachs and M. Dinkelmann, "Heat Input Reduction in Hypersonic Flight by Optimal Trajectory Control," AIAA Guidance Navigation and Control Conference, July 29-31, 1996 / San Diego, CA
- [7] Suhas V. Patankar, "Numerical Heat Transfer and Fluid Flow," Hemisphere Publishing Co. 1980.
- [8] David R. Olynick and Tim Tam, "Trajectory Based Validation of the Shuttle Heating Environment," AIAA Thermophysics Conference, June 17-20, 1996 / New Orleans, LA

Table 1 Flight Path Constraints

Constraint	Flight Parameter Constrained	TPS Type	Lower Limit	Upper Limit
<b>q</b>	Dynamic Pressure	all	20 psi	900 psi
<b>TSTAGN</b>	Stagnation temperature at vehicle nose	all	n/a	3000° F
<b>TLS</b>	Temperature lower surface	Tile	n/a	2400° F
		Blanket	n/a	2000° F
		Metallic	n/a	1800° F
<b>TUS</b>	Temperature upper surface	all	n/a	1200° F
<b>SLDFAC</b>	Load factor	all	0	2
<b>AN</b>	Vehicle angle of attack	all	-60°	+60°
<b>FA</b>	Vehicle flight path angle	all	-45°	+45°

Table 2 Comparison of Heat Transfer Equations in TEMP and HEATX

Subroutine	Input	Output	Boundary Condition @ Surface			B.C. @ H2 Tank	Thermal Capacitance	Material Properties
TEMP	QDOTconv	Tsurf	Conduction	Convection	Radiation	no terms	no terms	no terms
HEATX	QDOTconv dt Psurf Past T(x,t)	QDOTabs & T(x,t) of TPS	yes	yes	yes	Adiabatic Dry Wall	yes	c and k functions of T(x,t) & Psurf

Table 3 TPS Nodal Breakdown

TPS	Layer #	Material	# Nodes	Thickness Inches	Weight lb/ft^2
Tile	1	TUFI / AETB12	5	0.1	0.500
	2	AETB12	5	2	2.008
	3	RTV - 560	1	0.012	0.088
	4	Aluminum	1	0.08	1.167
	<b>Total</b>		<b>12</b>	<b>2.192</b>	<b>3.763</b>
Blanket	1	TABI	5	2	1.550
	2	RTV - 560	1	0.012	0.088
	3	Aluminum	1	0.08	1.167
	<b>Total</b>		<b>7</b>	<b>2.092</b>	<b>2.805</b>
Metallic	1	Inconel 617 Honeycomb Sandwich	5	0.29	0.628
	2	Q - Fiber Felt	5	3.5	1.020
	3	Titanium Honeycomb Sandwich	1	0.18	0.363
	4	Air (gap)	1	0.5	n/a
	5	Aluminum	1	0.08	1.167
	<b>Total</b>		<b>13</b>	<b>4.55</b>	<b>3.178</b>

Table 4 Comparison of Optimization Functions

Case #	PHIDOT	Phi	Flight Time @ Landing	Descent Time Min	Trajectory Type	Max Structure Temperature Tile	Blanket	F Metallic
1	QDOTabs @ surface	Qabs @ surface	297	42	min. Q	271	267	353
2	T <sup>4</sup> 4	S T <sup>4</sup> 4 dt	288	33	min. Q	255	253	329
3	n/a does not employ ESA technique	n/a	295	40	min. Q	272	271	355
4	QDOTabs @ tank	Qabs @ tank	281	26	max. Q	267	287	337
5	QDOTabs @ tank	Qabs @ tank	271	16	max. Q	230		

**Figure 1**

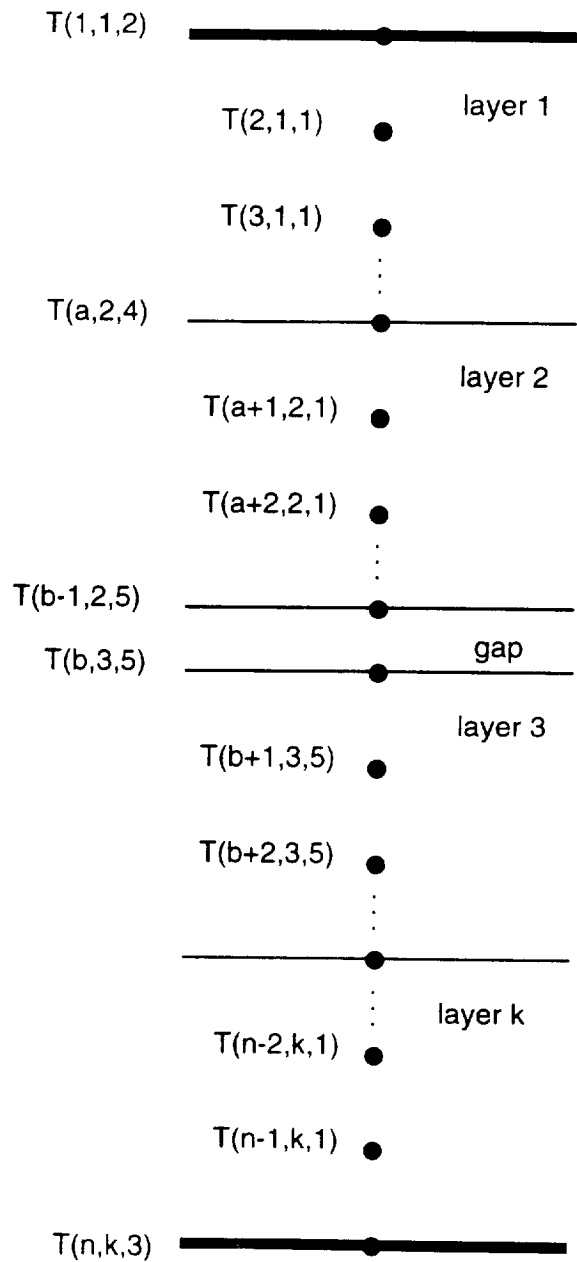
**Nodal Types**

- 1 Inner Layer
- 2 TPS Surface Boundary
- 3 TPS Tank Boundary
- 4 Layer Boundary
- 5 Layer Boundary w/gap

**Variables**

- $k$  = total # of layers in TPS
- $n$  = total # of nodes in TPS
- $a$  = first node in layer 2
- $b$  = first node in layer 3

**T(Node #, Layer #, Type#)**





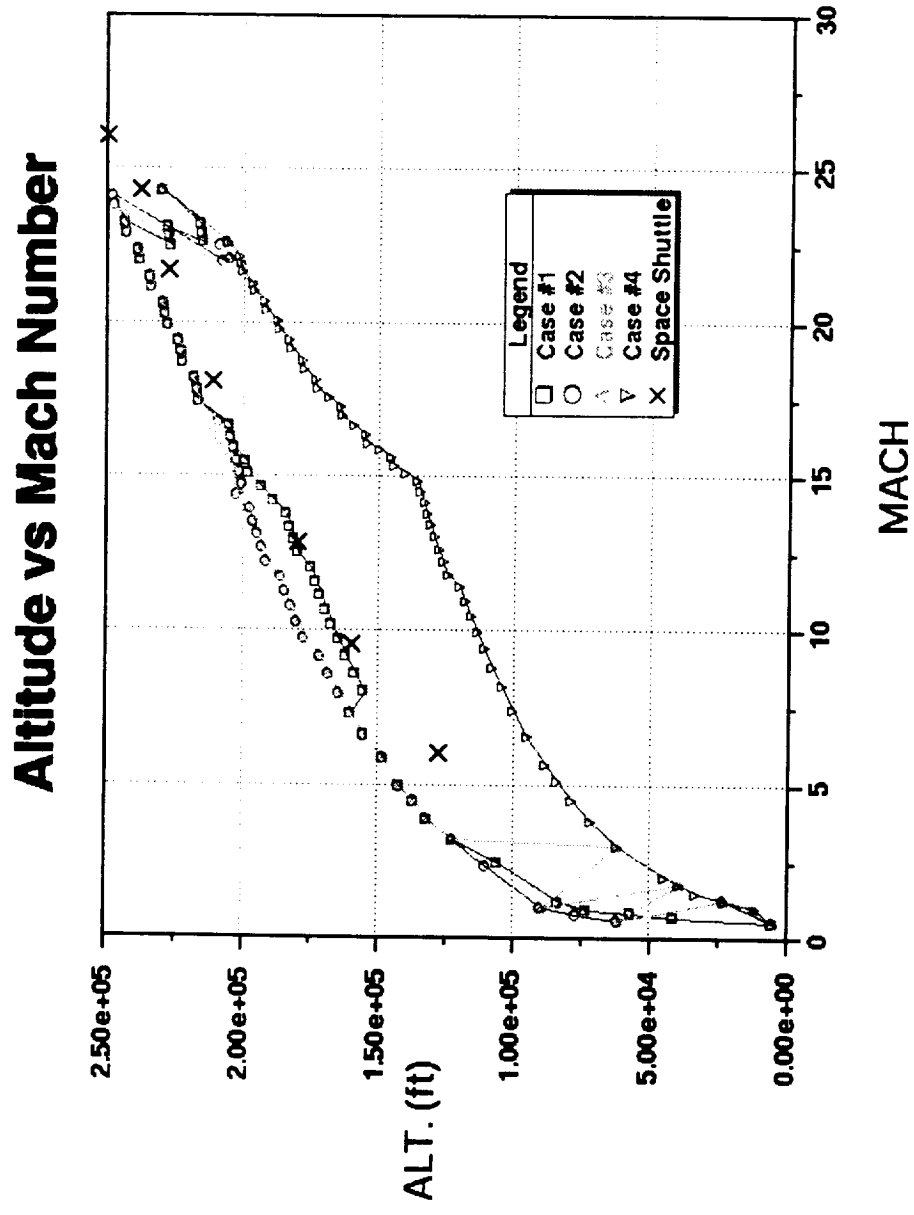


Figure 2

# QDOTconv vs FLIGHT TIME

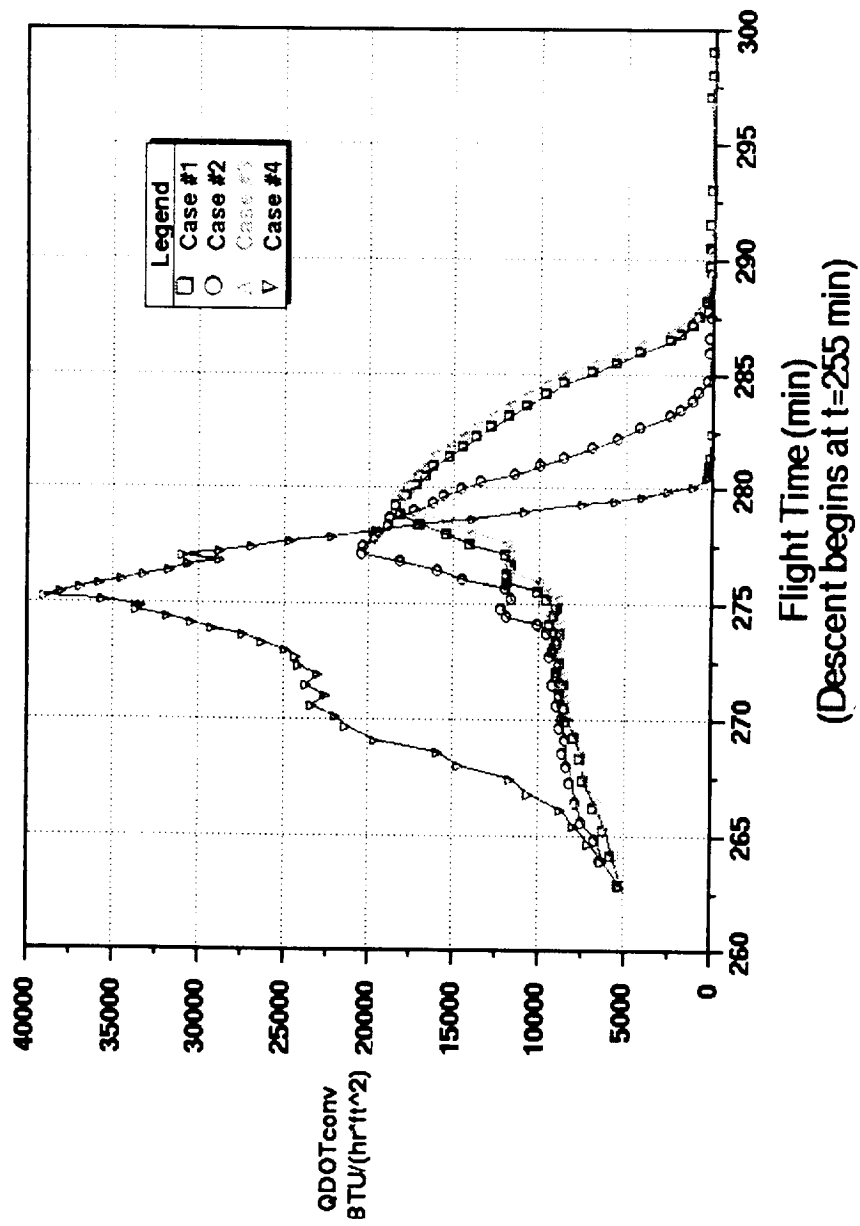


Figure 3

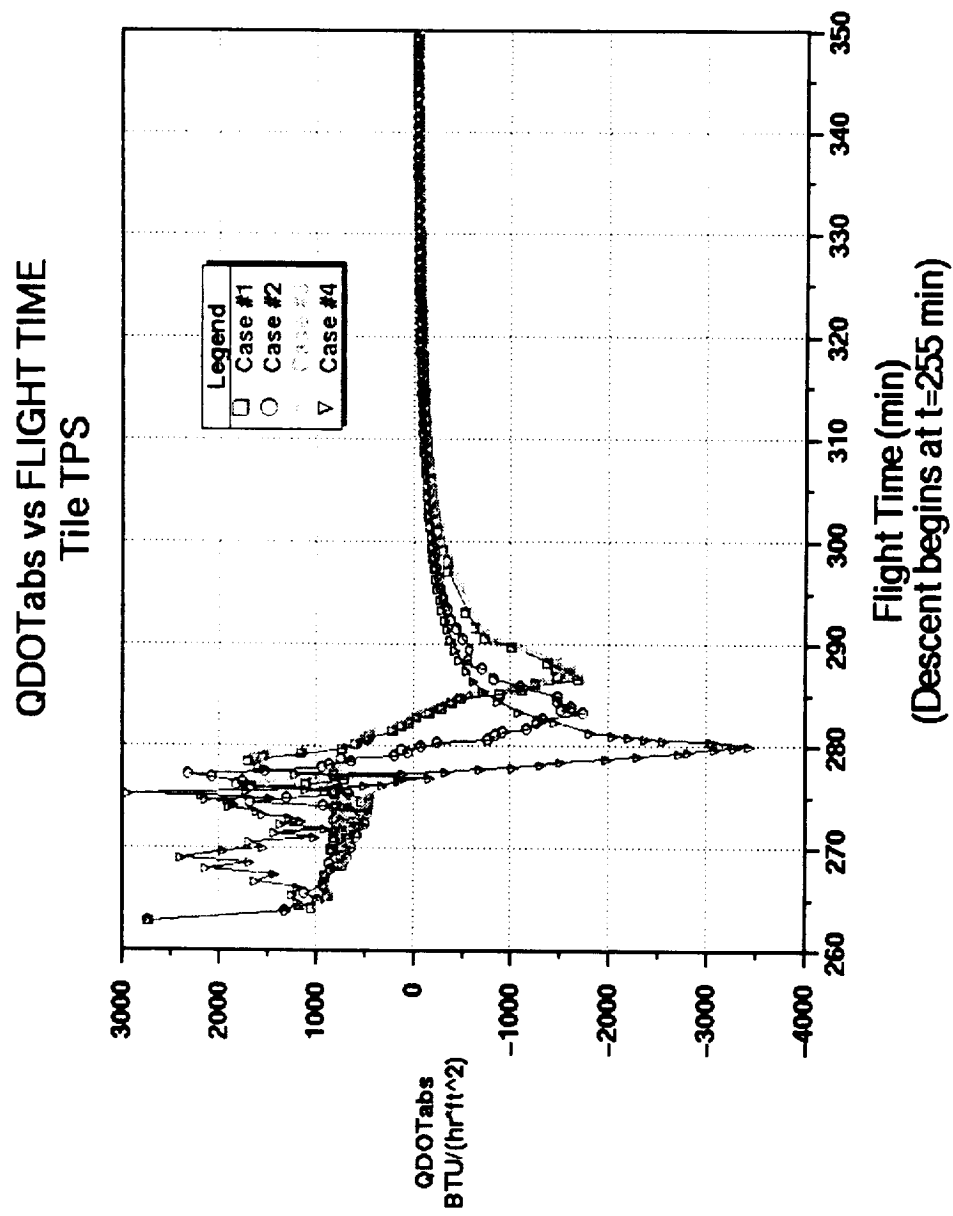


Figure 4.1

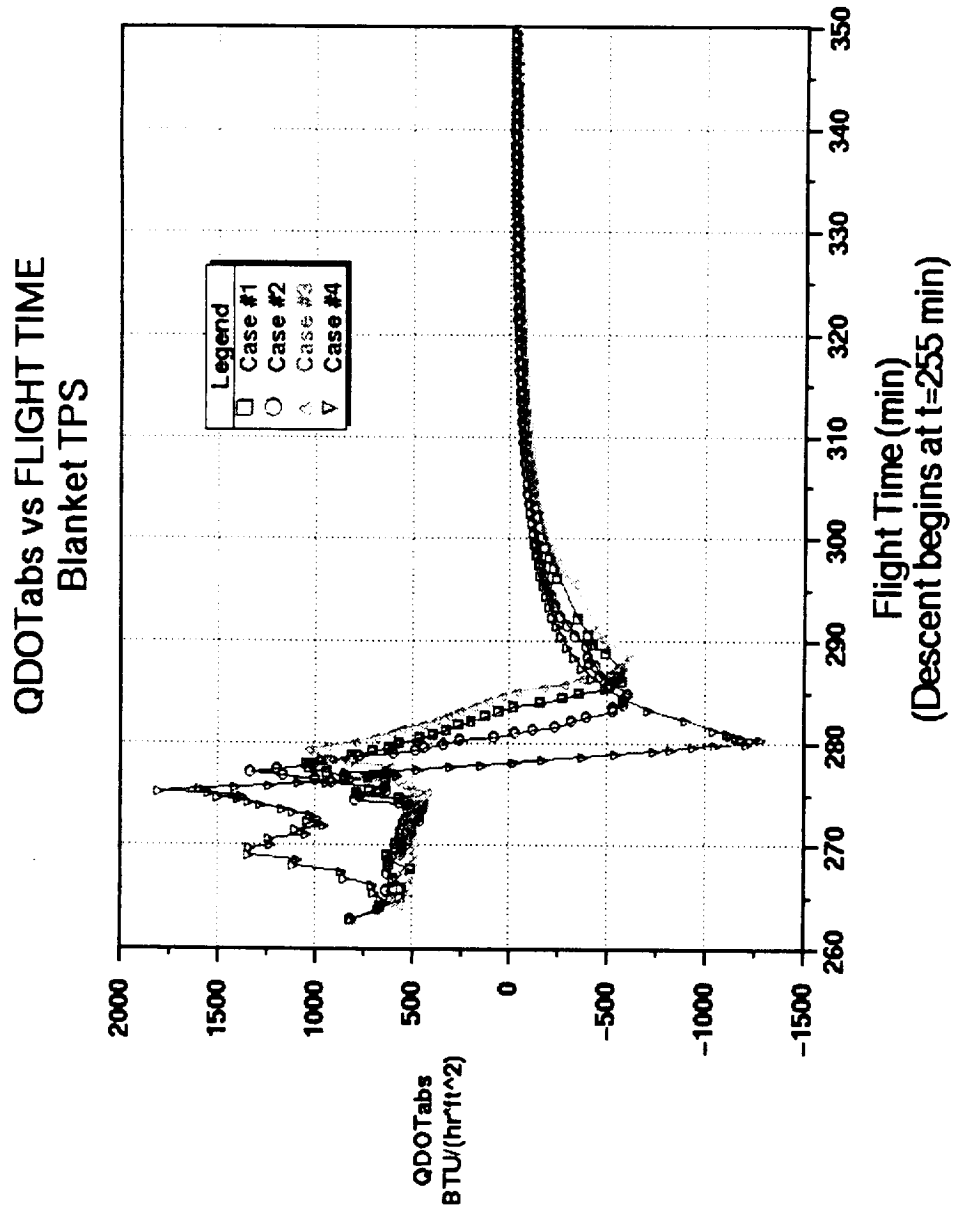


Figure 4.2

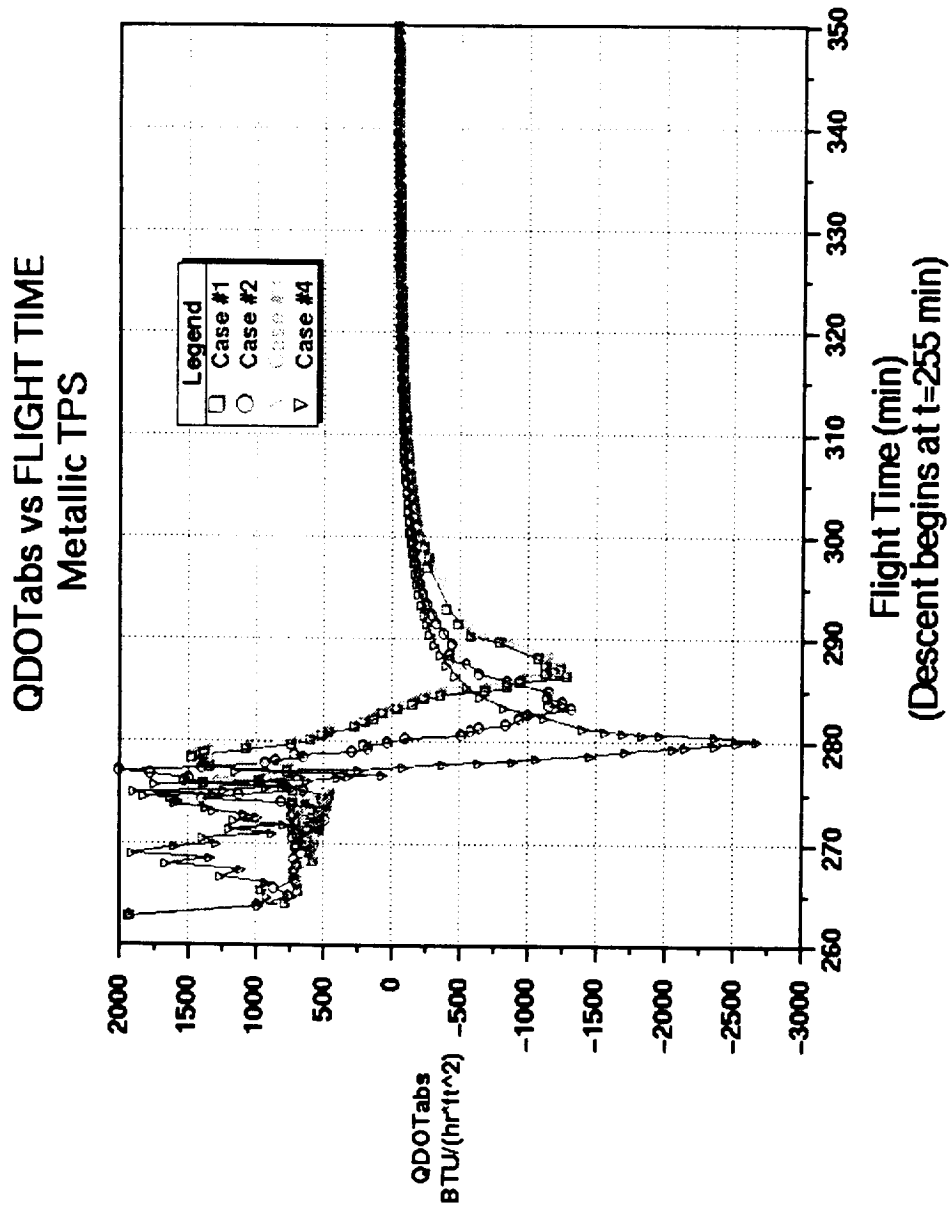


Figure 4.3

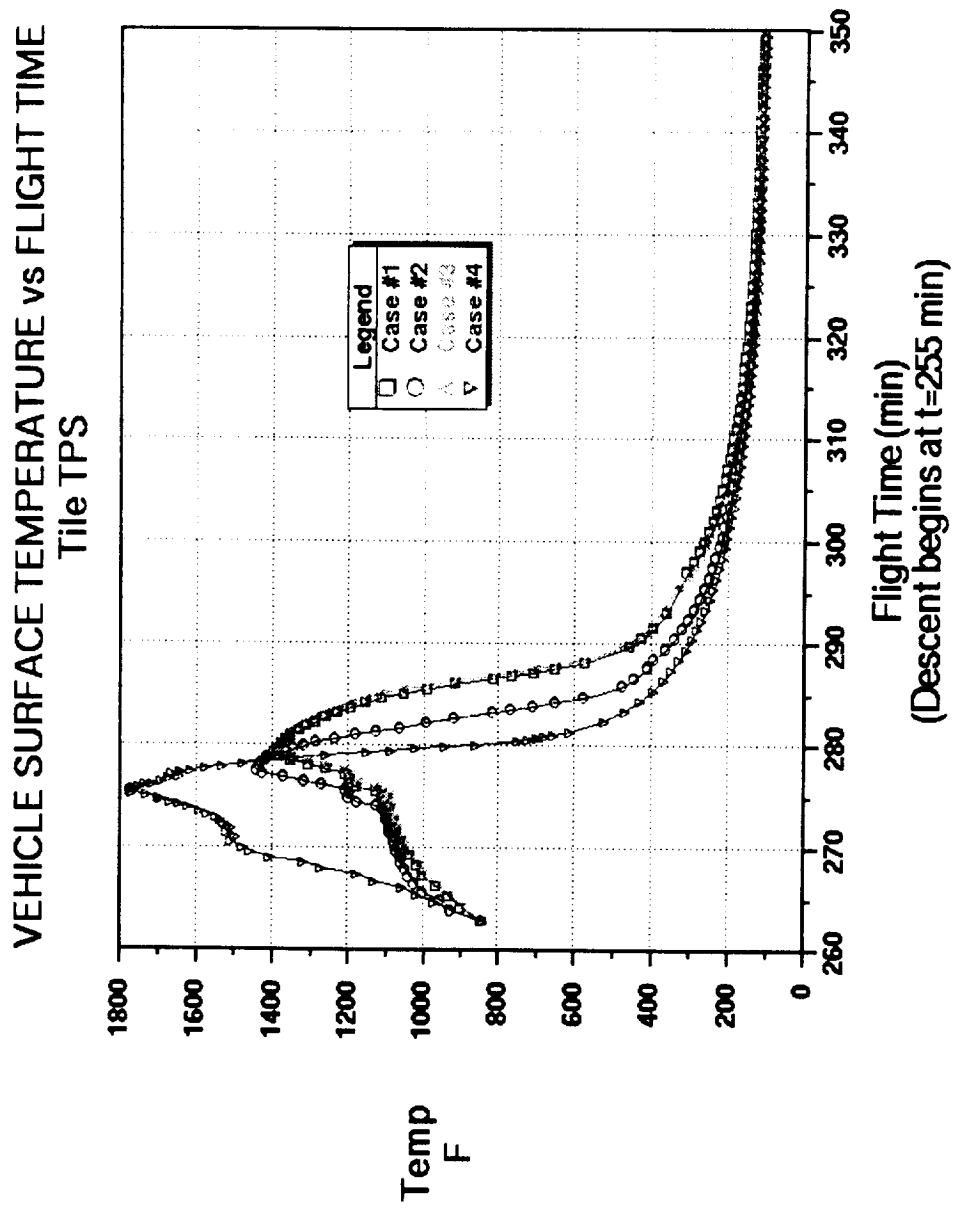


Figure 5.1

# VEHICLE SURFACE TEMPERATURE vs FLIGHT TIME Blanket TPS

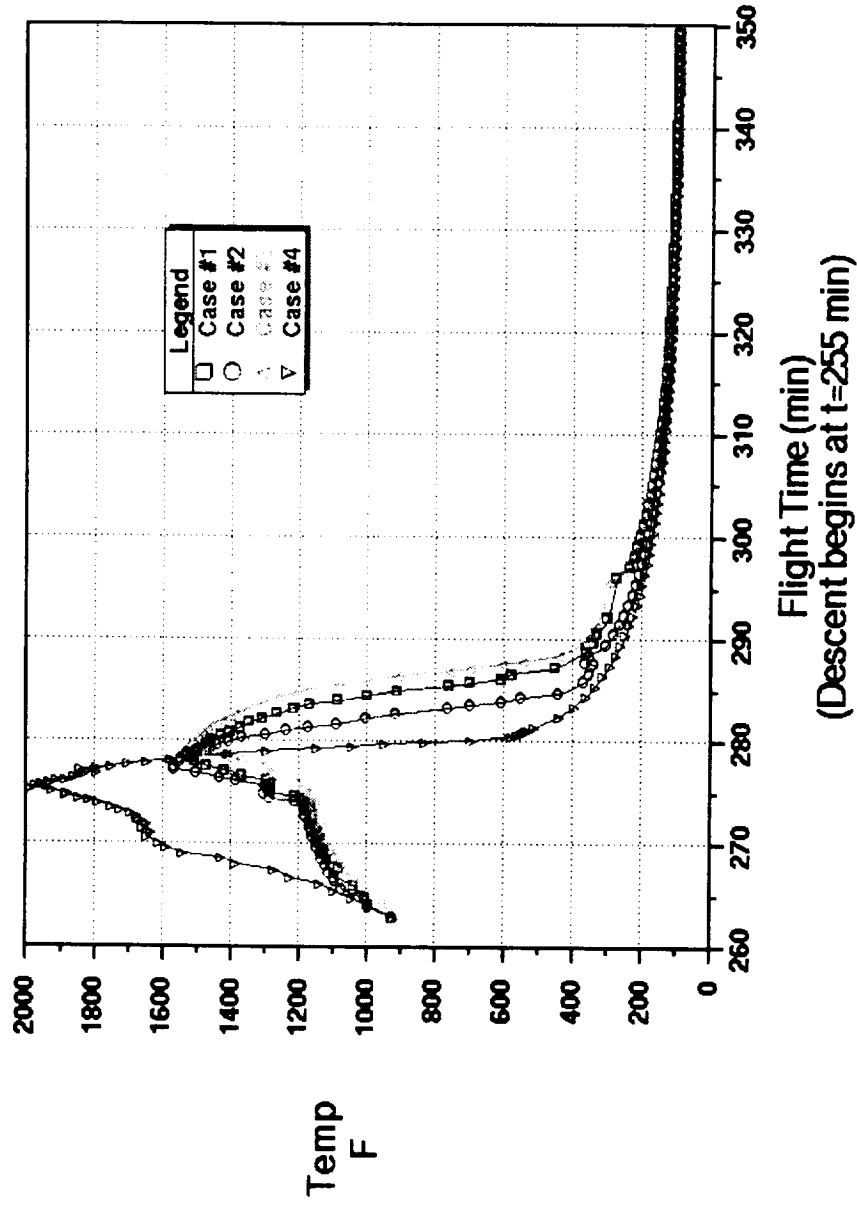


Figure 5.2

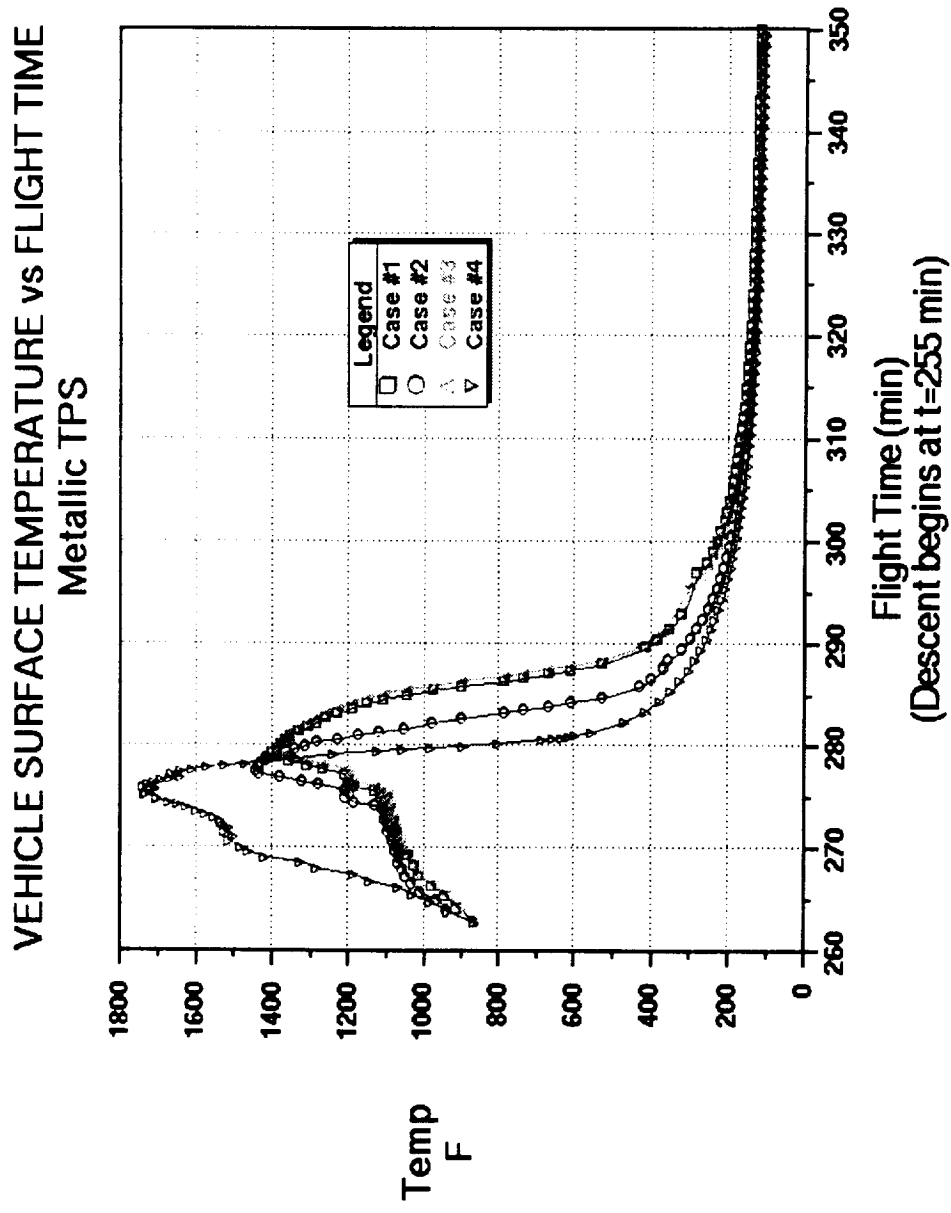


Figure 5.3



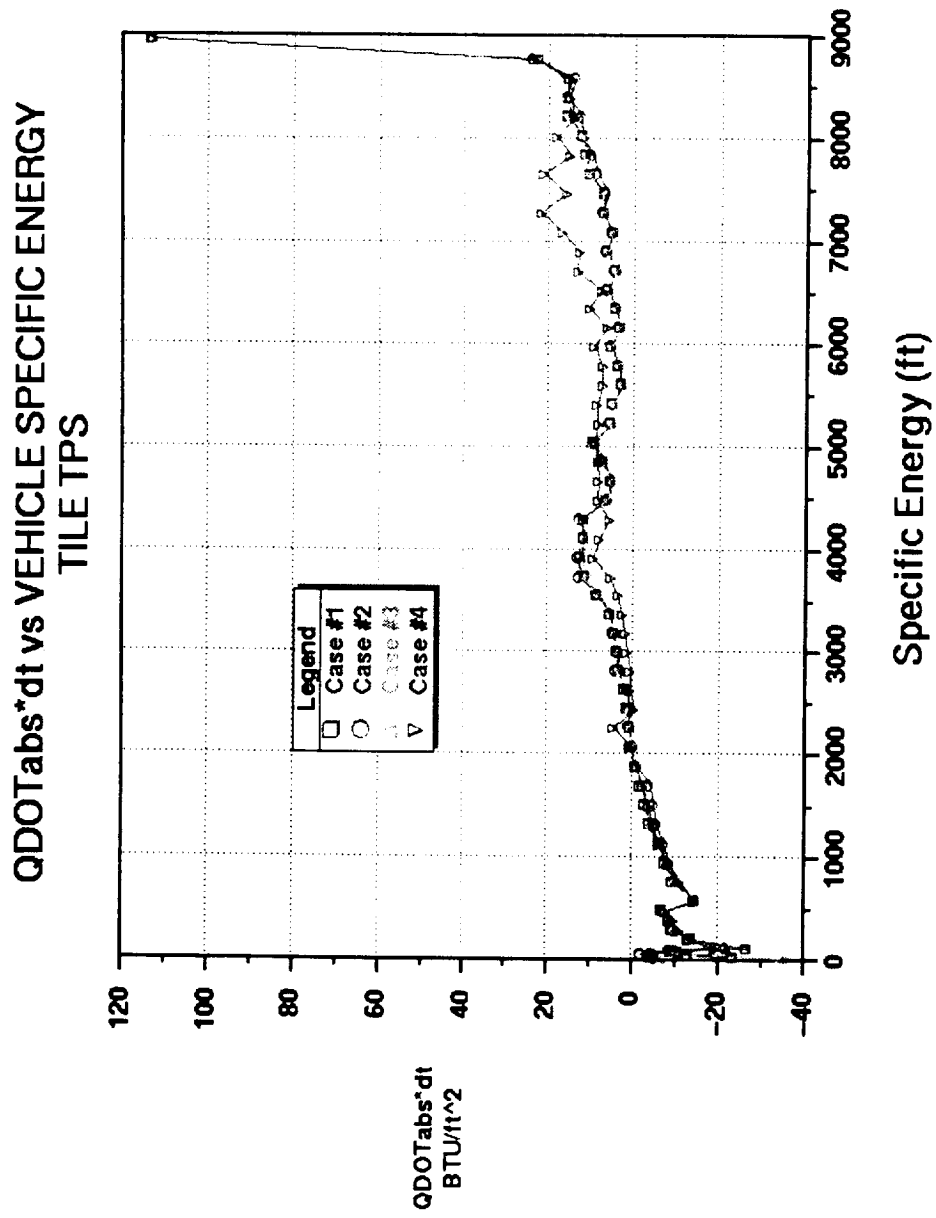


Figure 6.1

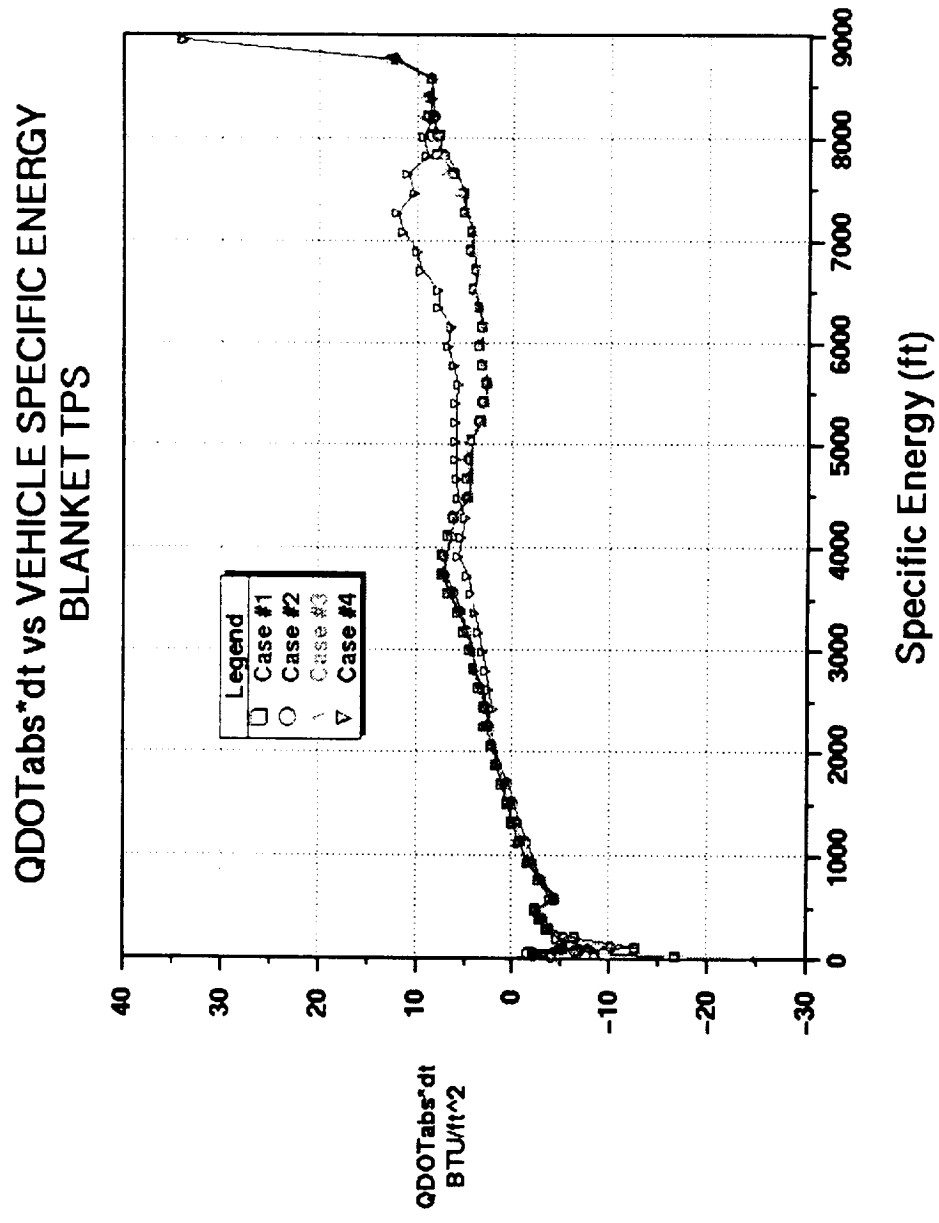


Figure 6.2

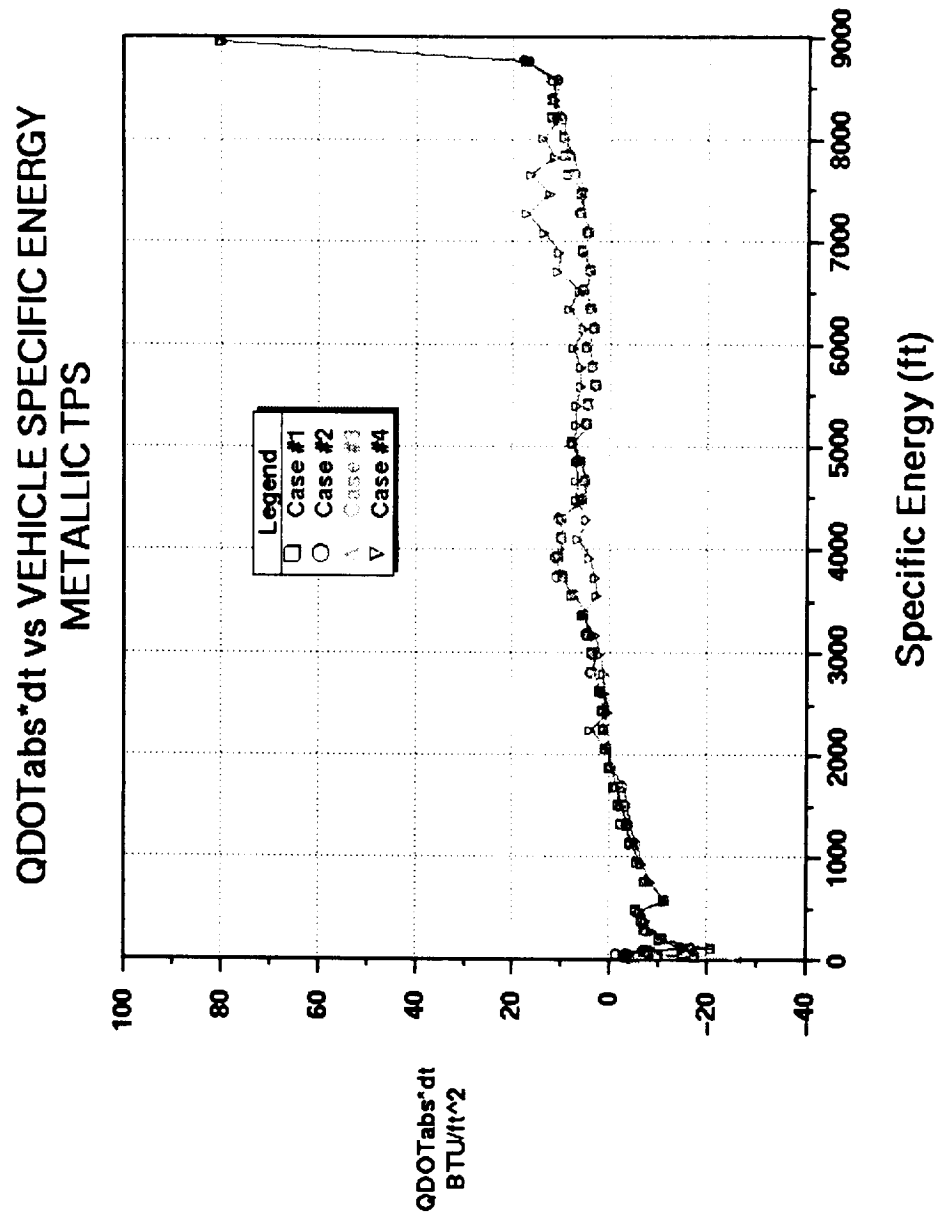


Figure 6.3

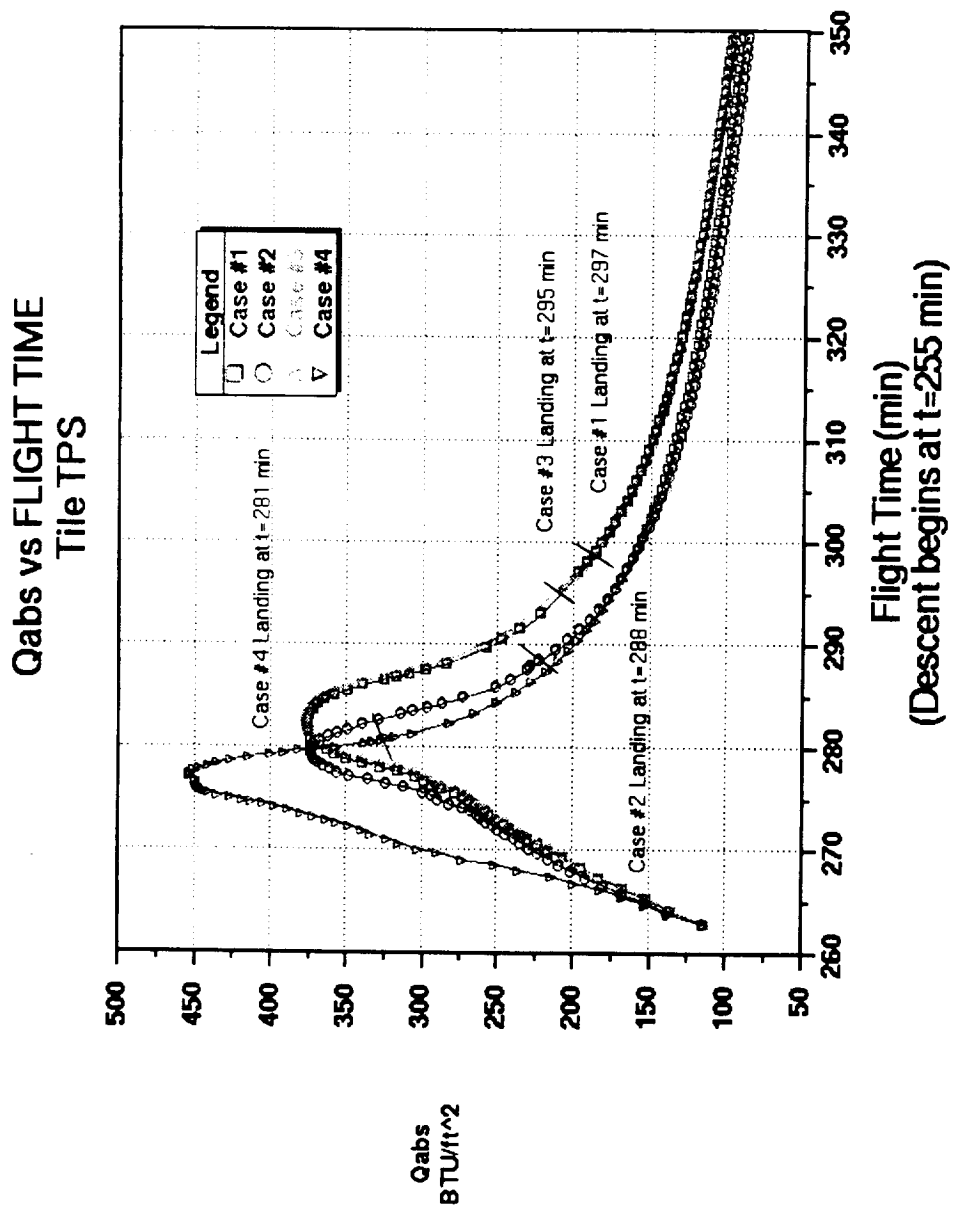


Figure 7.1

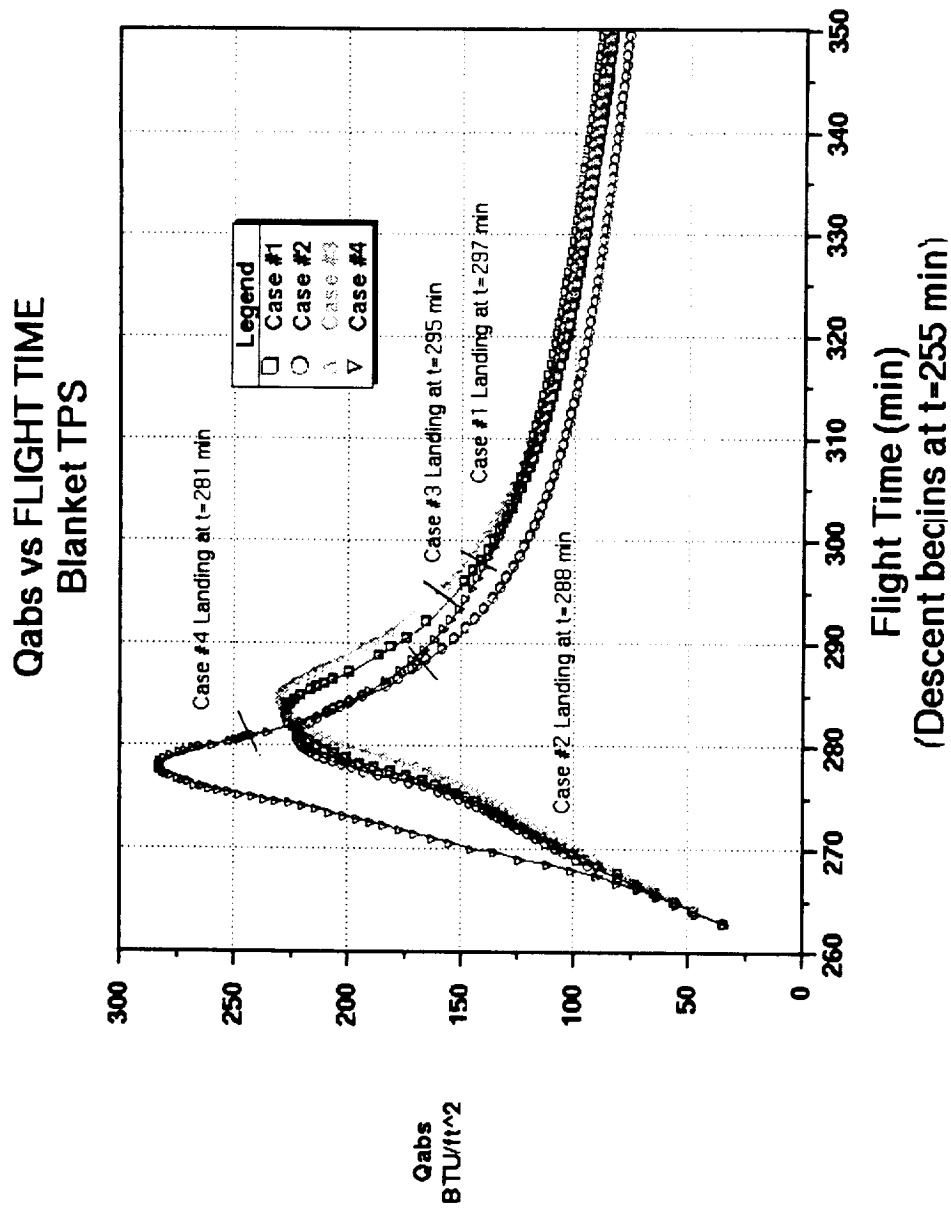


Figure 7.2

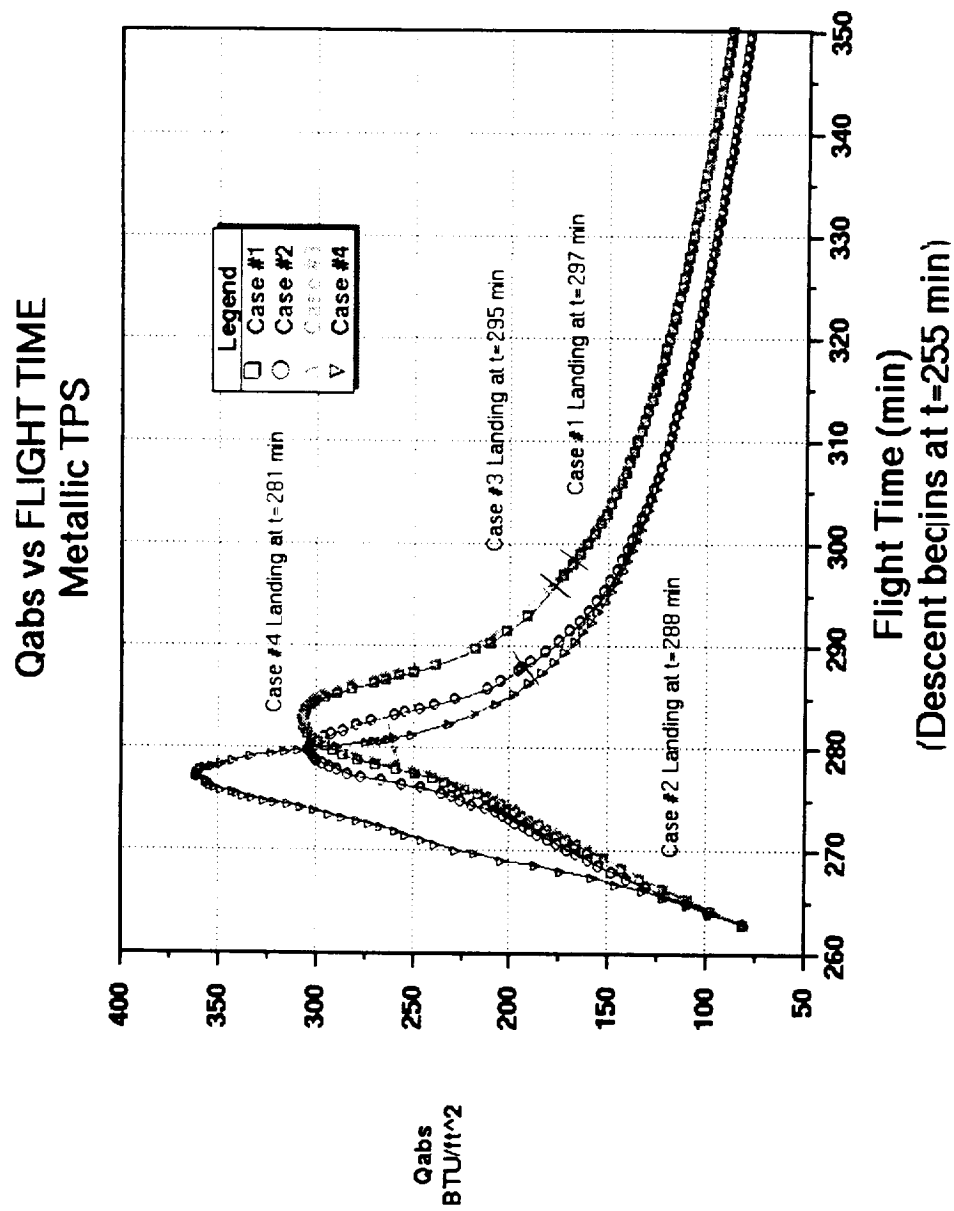


Figure 7.3

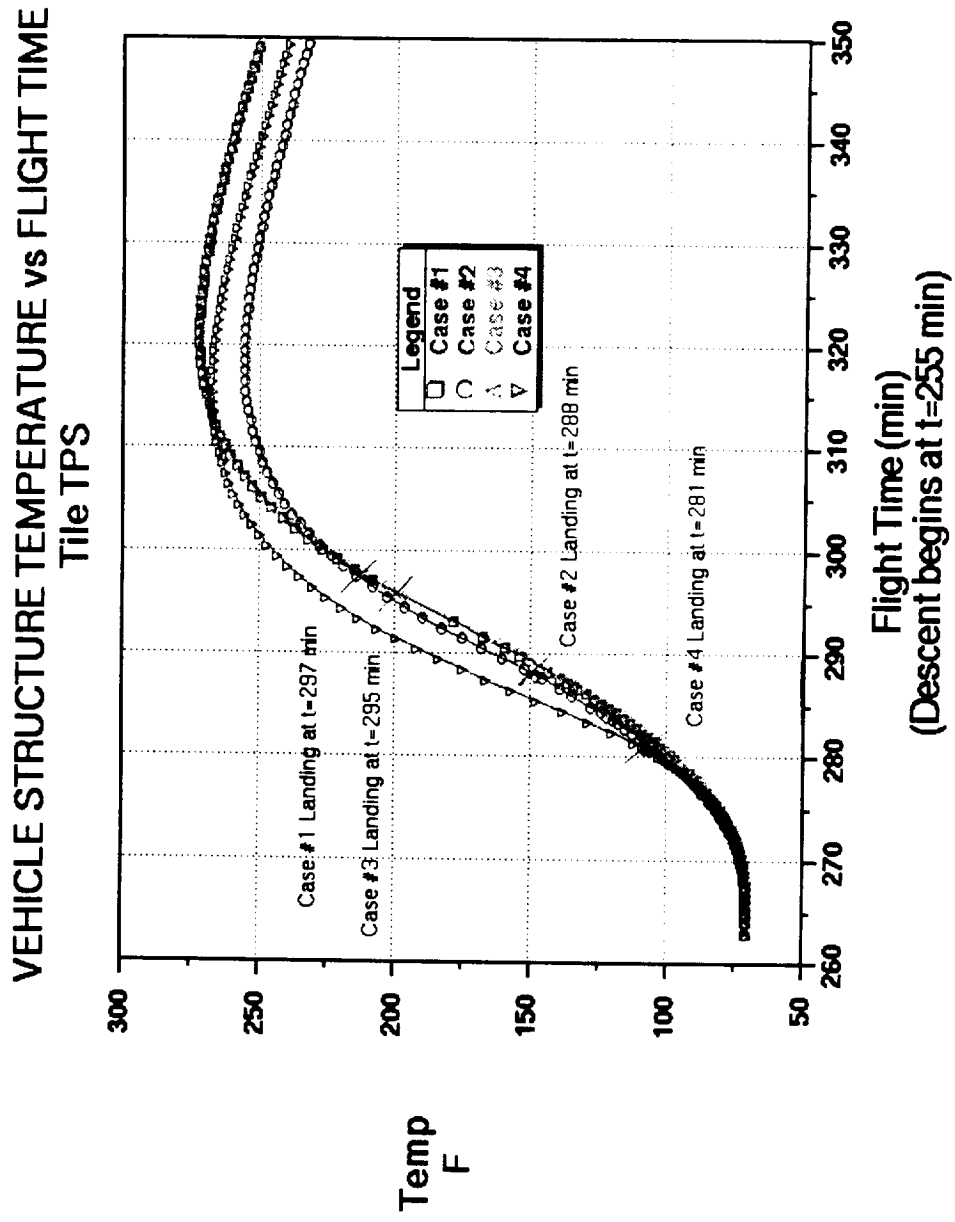


Figure 8.1

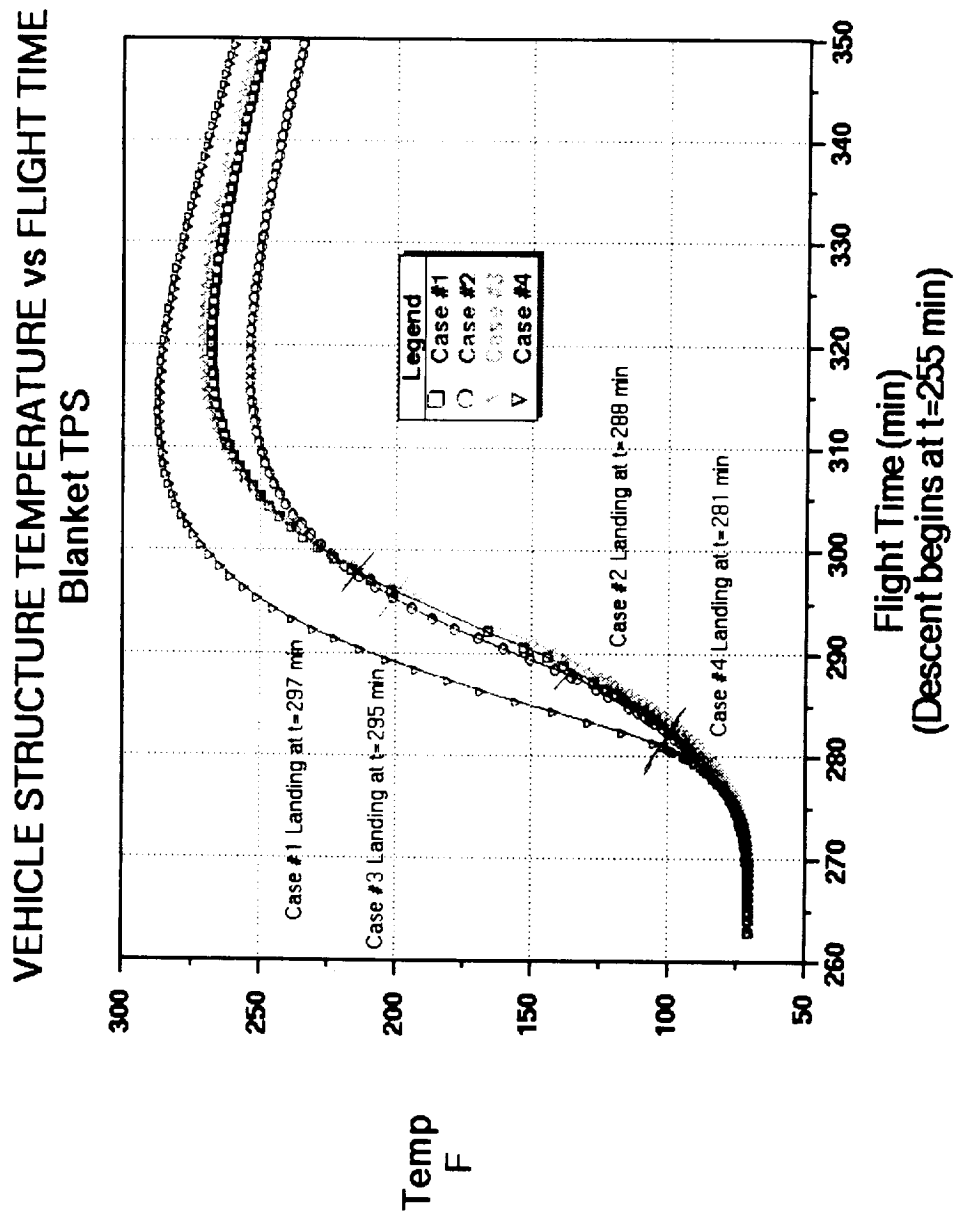


Figure 8.2



# VEHICLE STRUCTURE TEMPERATURE vs FLIGHT TIME Metallic TPS

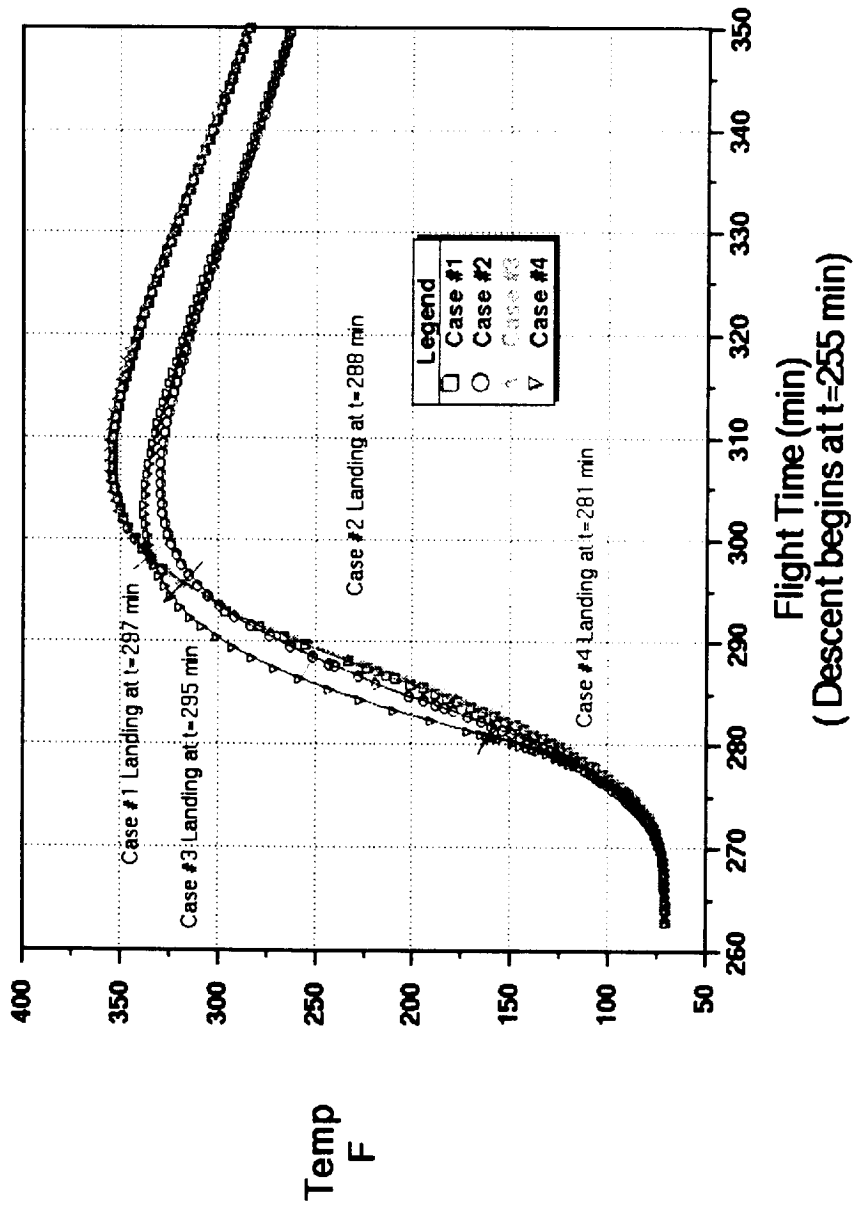


Figure 8.3

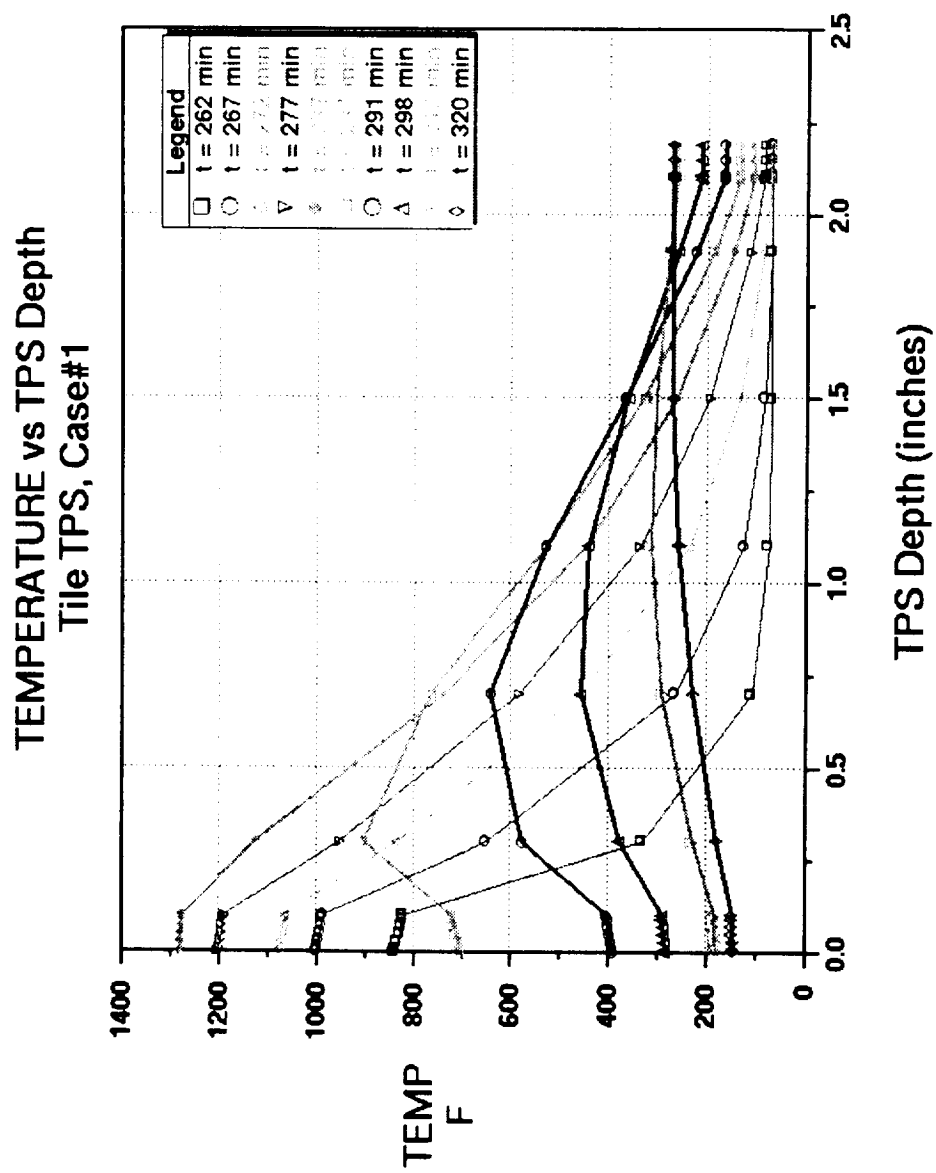


Figure 9

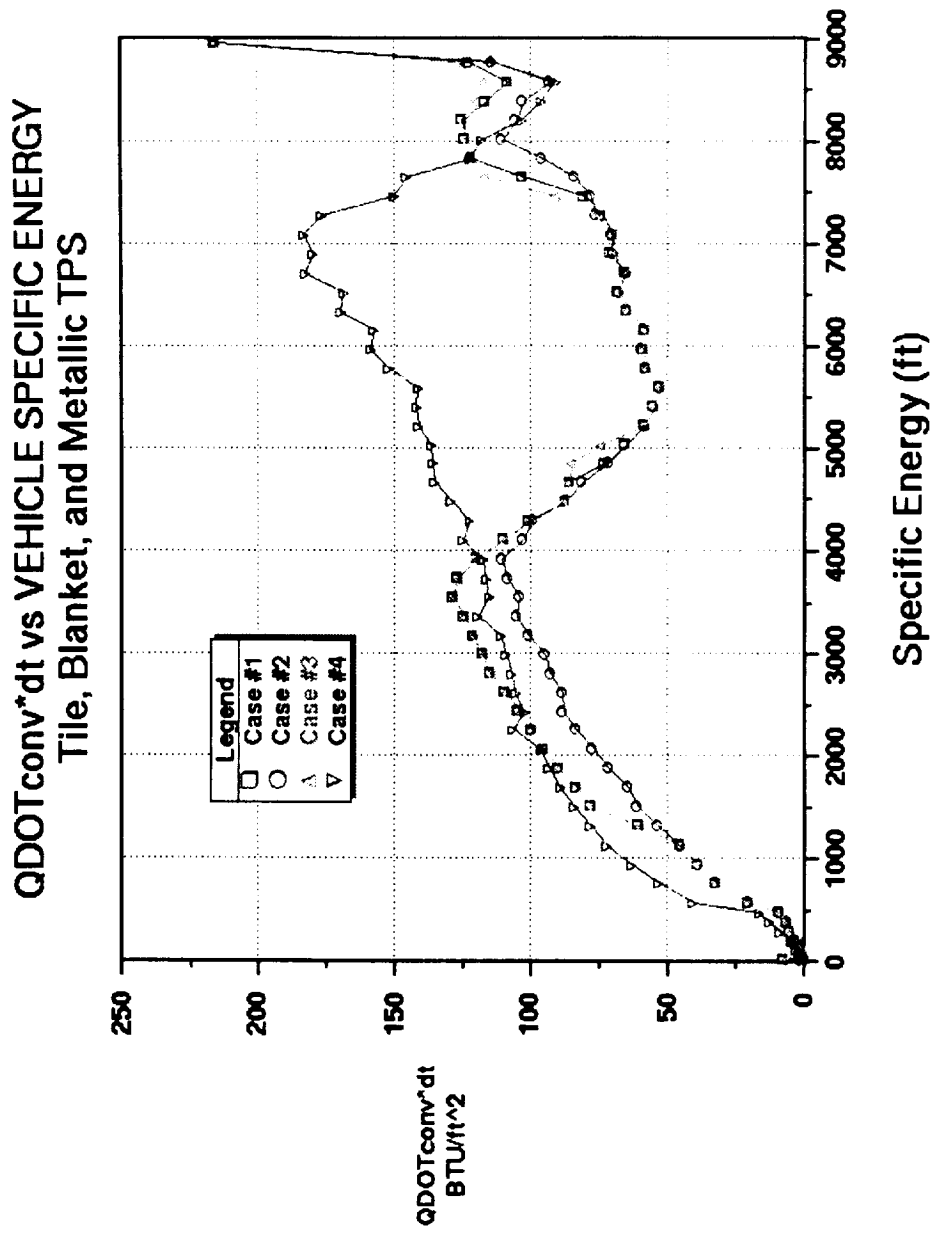


Figure 10

# Qconv vs FLIGHT TIME

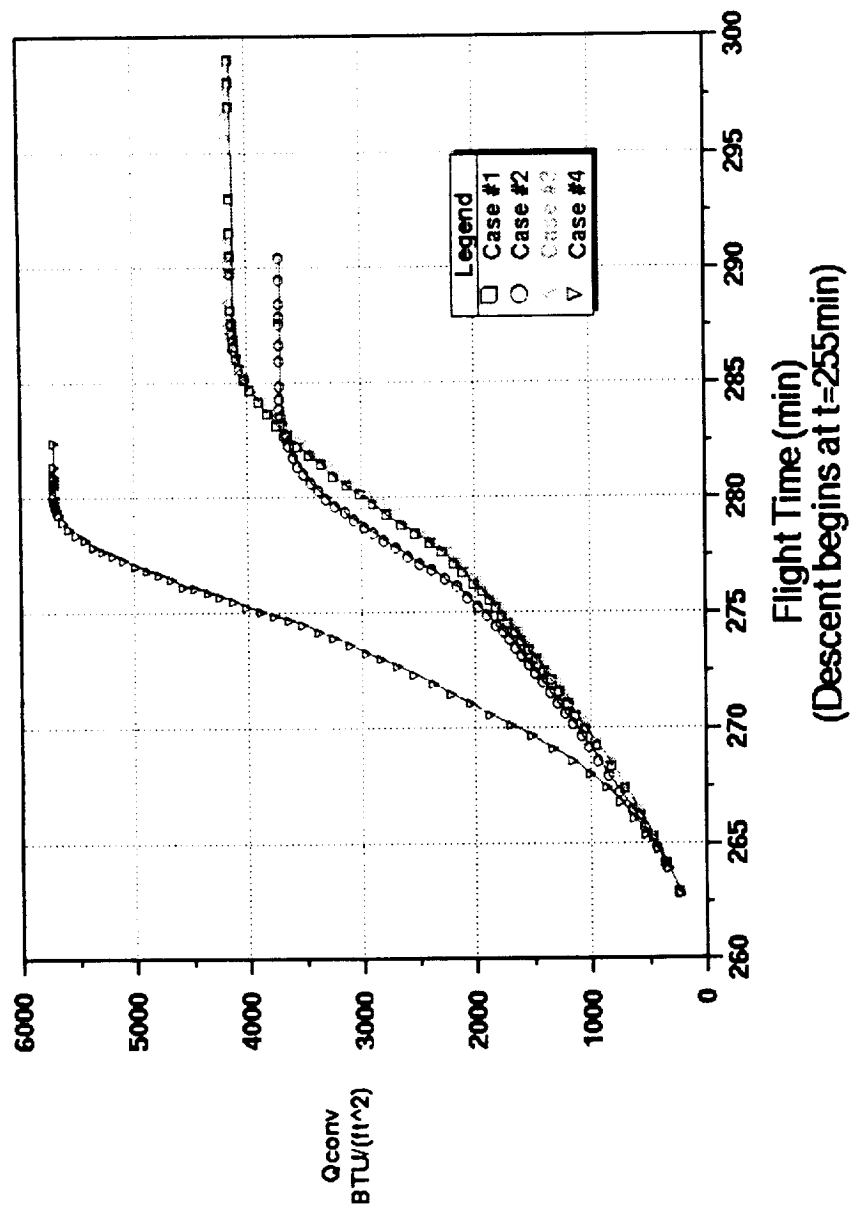


Figure 11

# TEMPERATURE LOWER SURFACE vs VEHICLE SPECIFIC ENERGY Tile, Blanket, and Metallic TPS

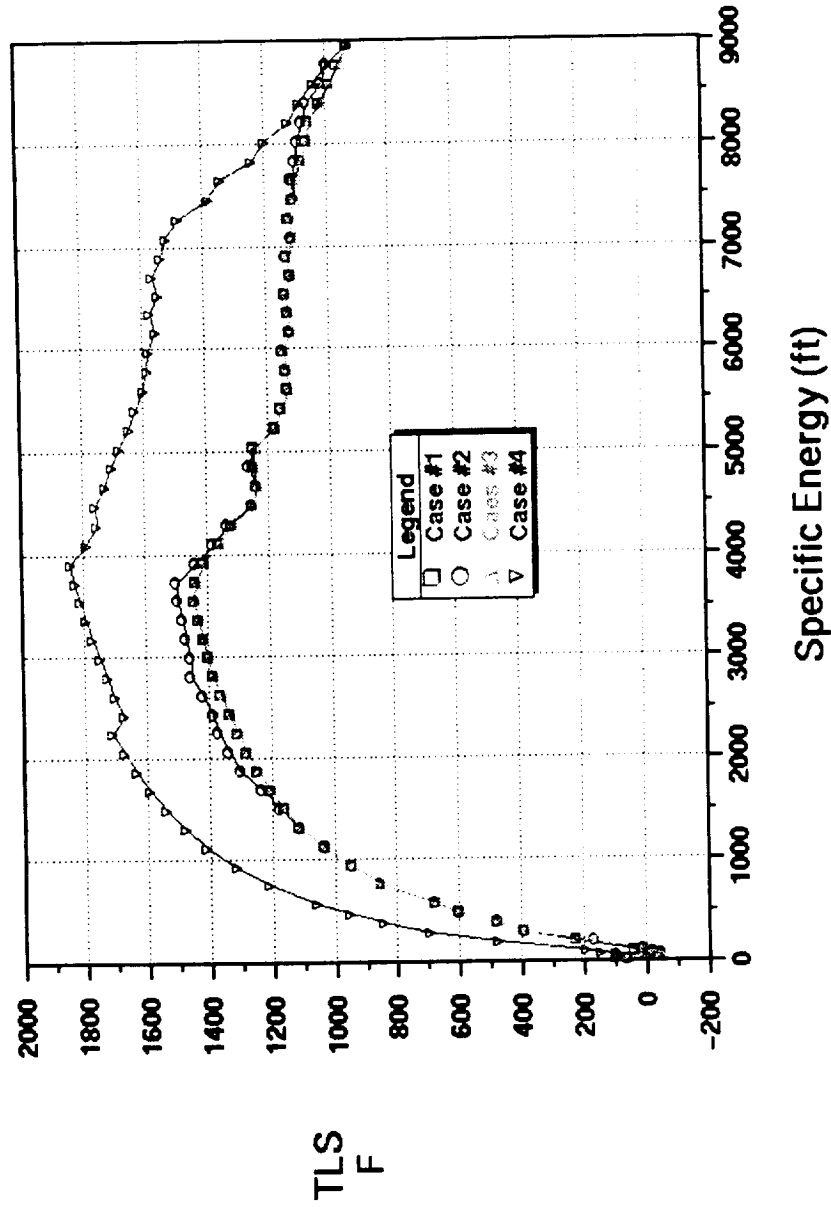


Figure 12

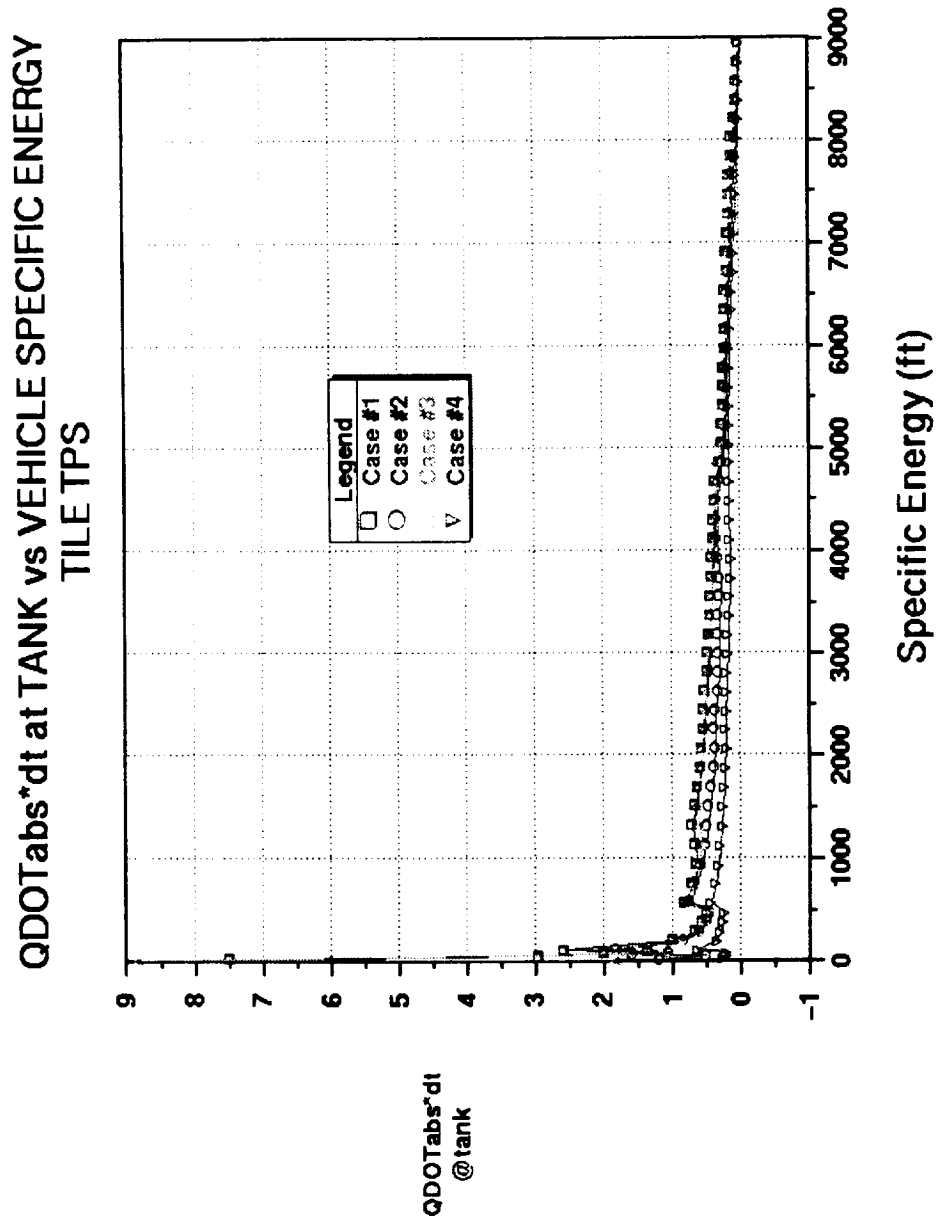


Figure 13.1

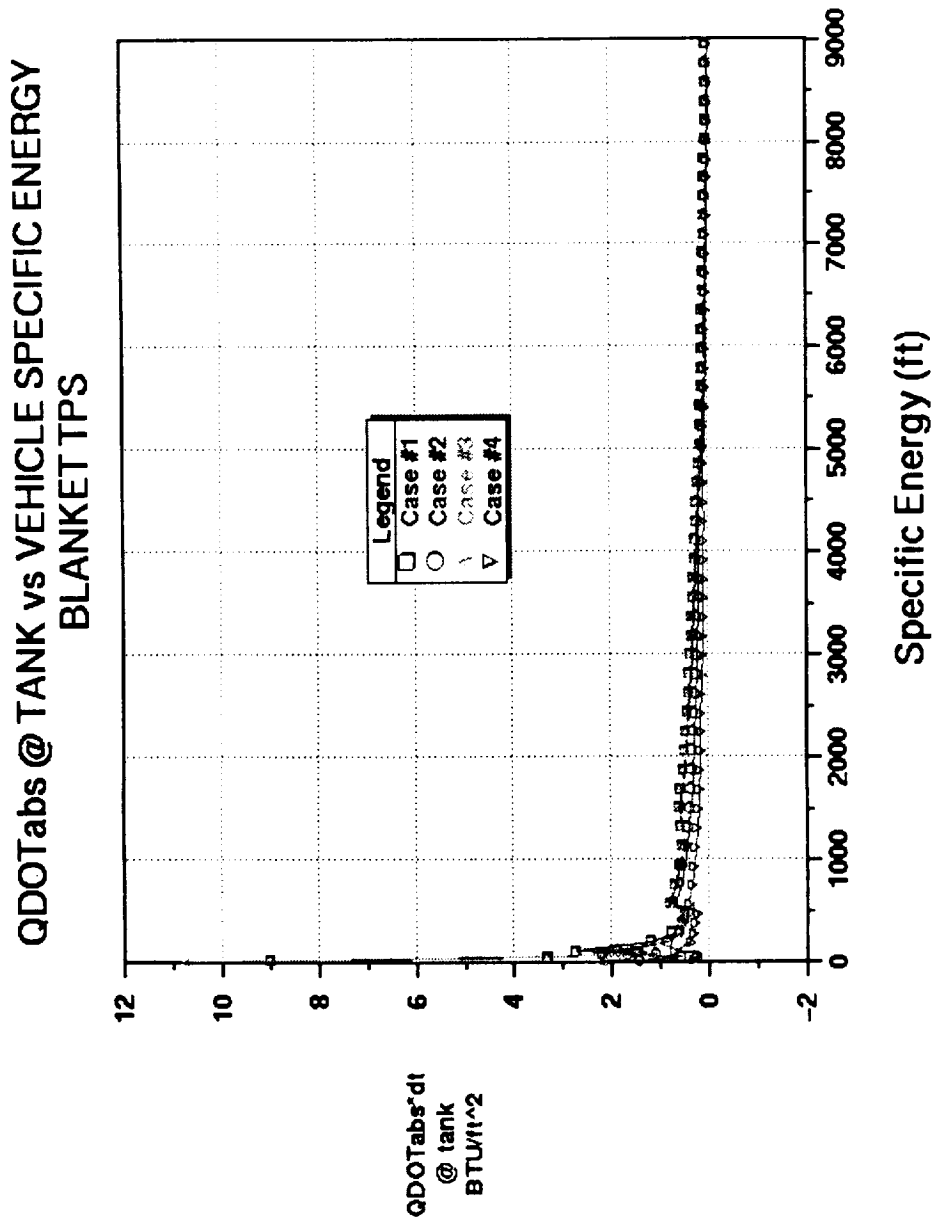


Figure 13.2

# QDOTabs\*dt @ TANK vs VEHICLE SPECIFIC ENERGY METALLIC TPS

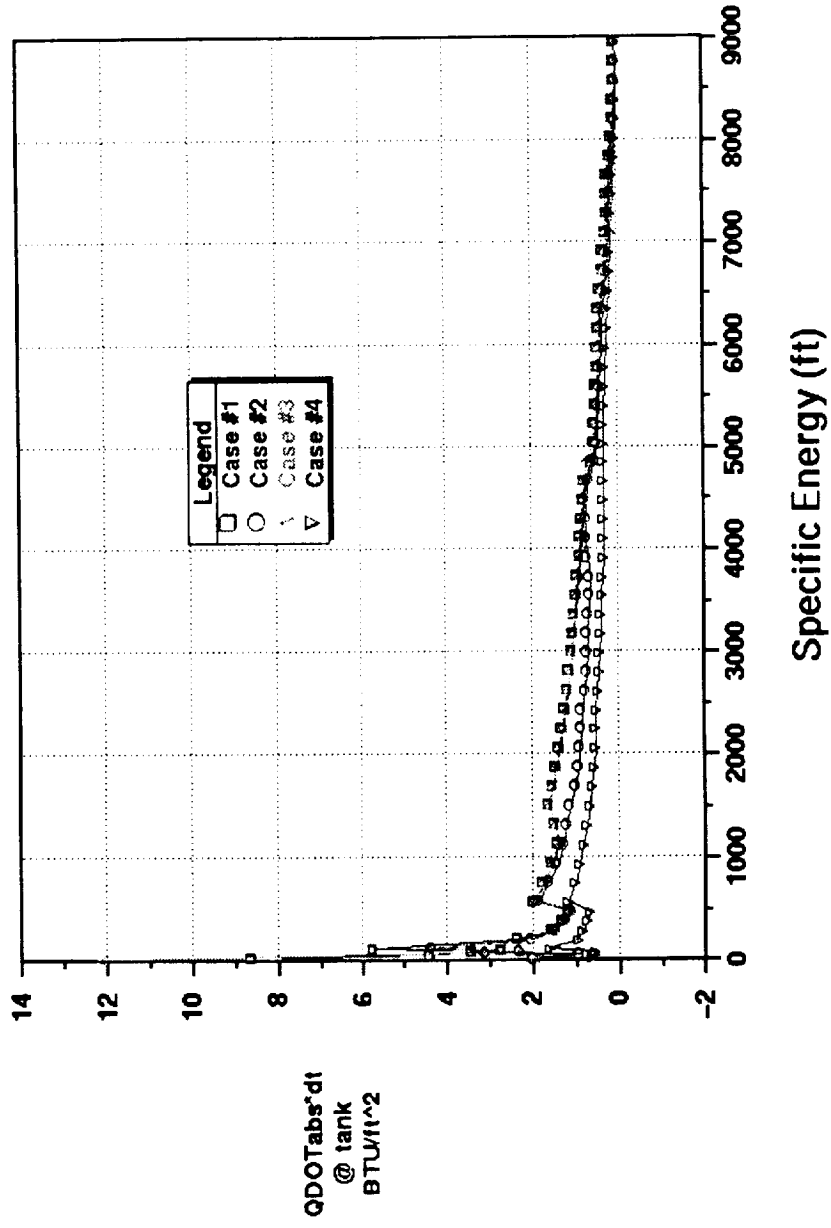


Figure 13.3



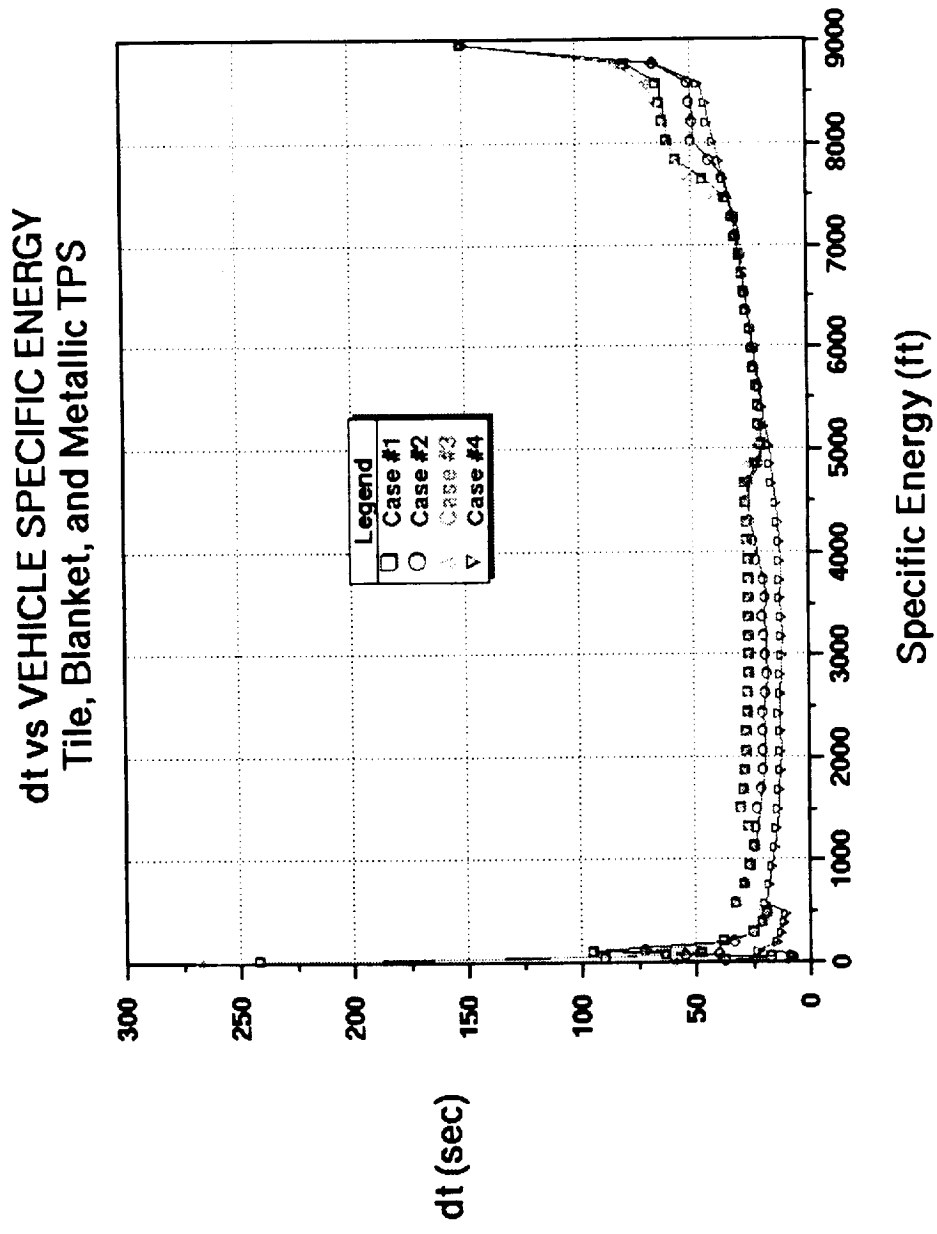


Figure 14

## ALT. vs MACH

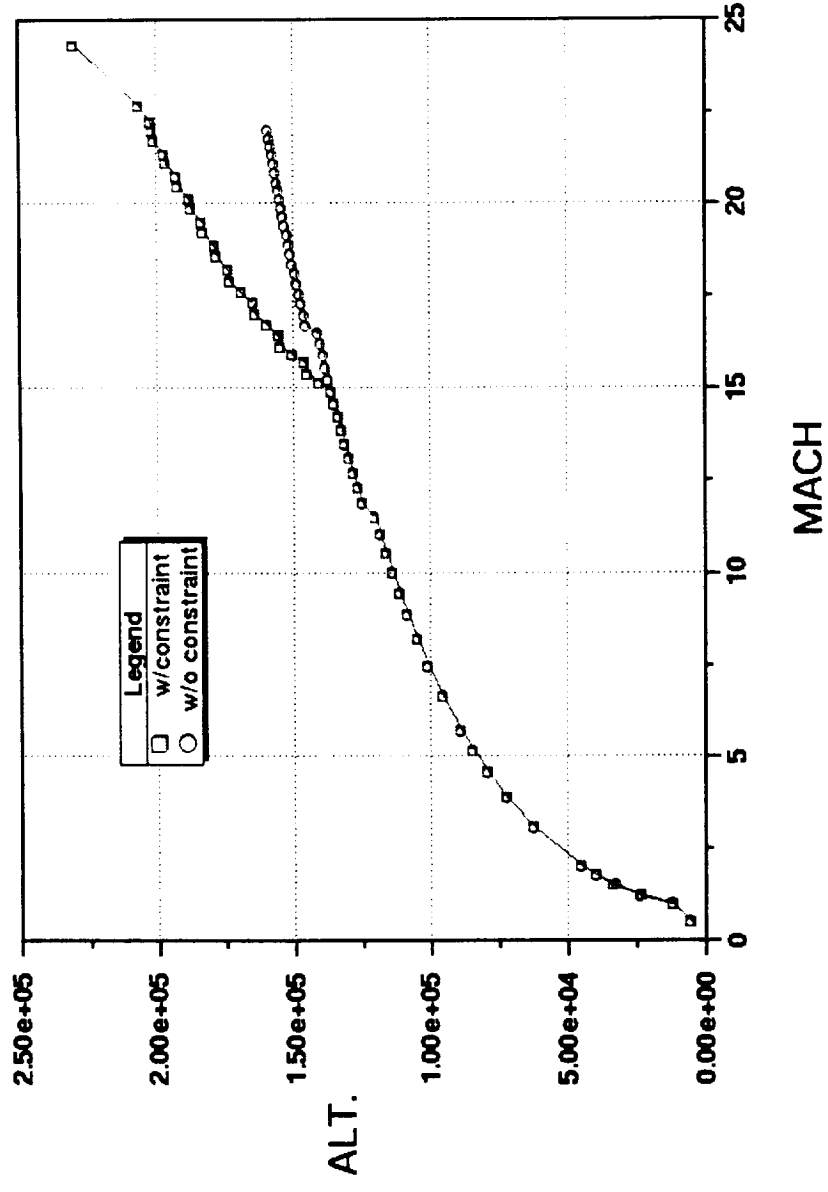


Figure 15

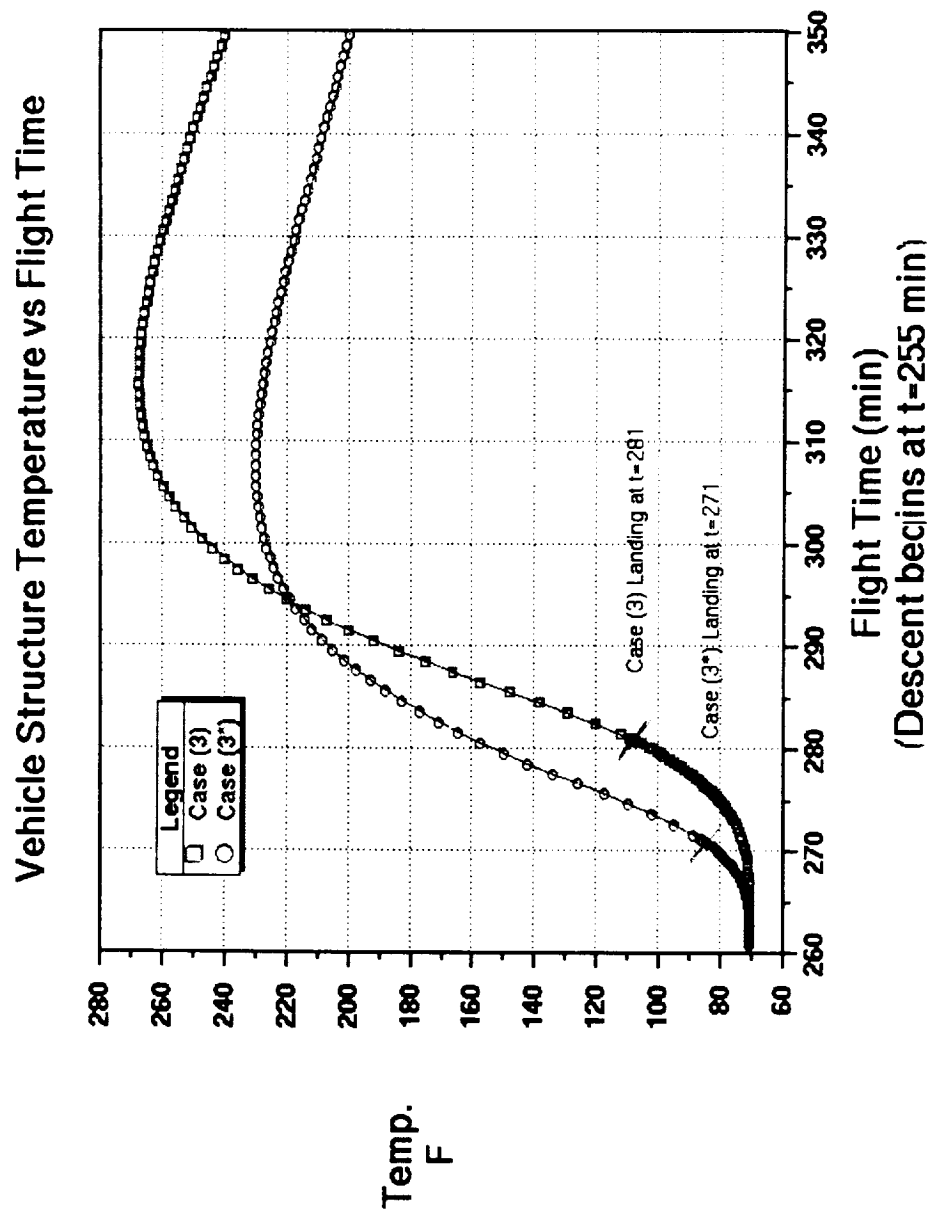


Figure 16

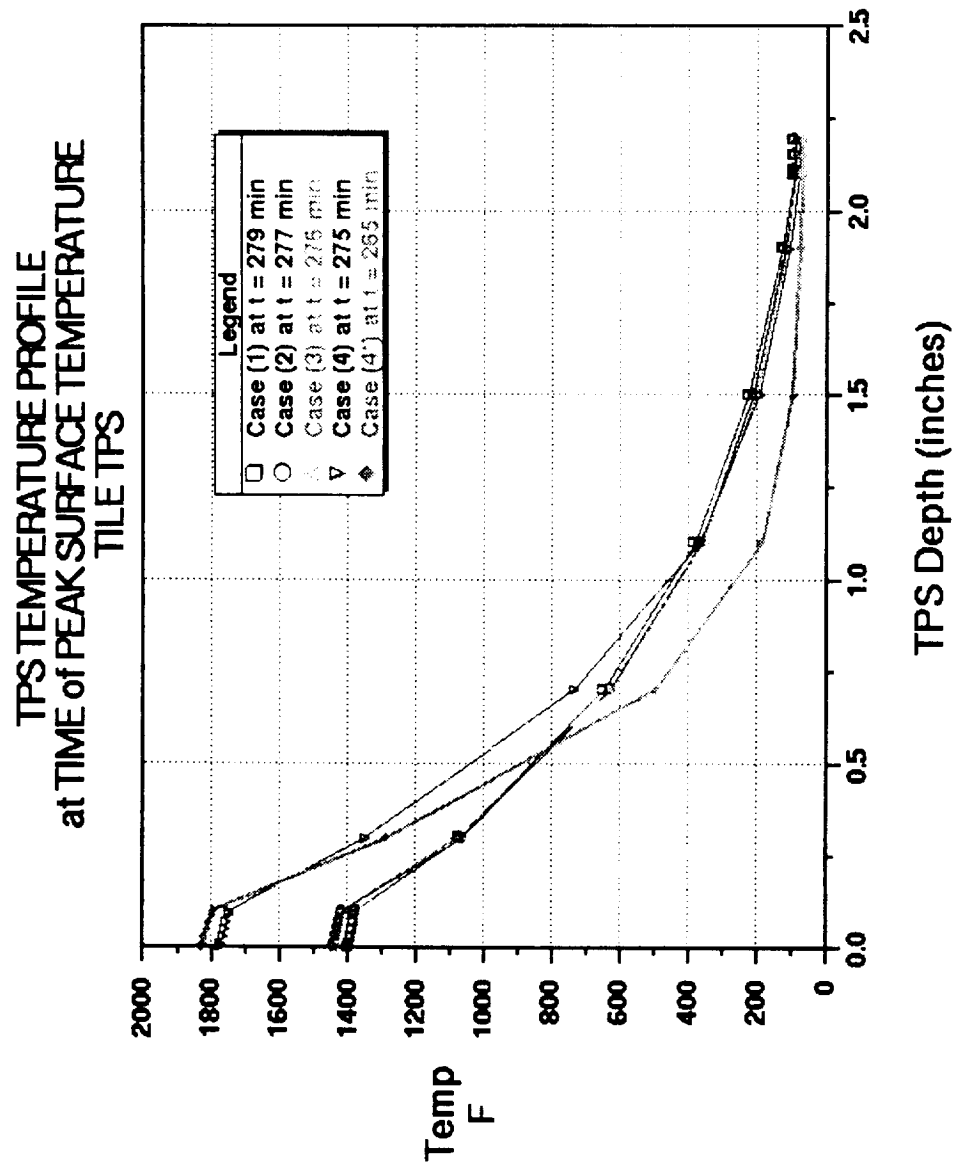


Figure 17

**SANTA CLARA UNIVERSITY**

Department of Mechanical Engineering

February 5, 1997

I HEREBY RECOMMEND THAT THE THESIS PREPARED  
UNDER MY SUPERVISION BY

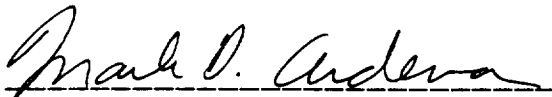
ROBERT WINDHORST

ENTITLED

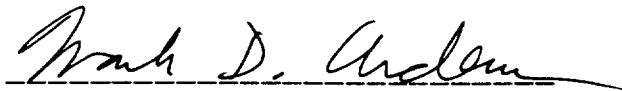
**Minimum Heating Re-Entry Trajectories for  
Advanced Hypersonic Launch Vehicles**

BE ACCEPTED IN PARTIAL FULFILLMENT OF THE REQUIREMENTS  
FOR THE DEGREE OF

**MASTERS OF SCIENCE  
IN  
MECHANICAL ENGINEERING**

A handwritten signature in cursive script, reading "Mark D. Ardema", written over a horizontal line.

Dr. Mark Ardema  
Thesis Advisor

A handwritten signature in cursive script, reading "Mark D. Ardema", written over a horizontal line.

Dr. Mark Ardema  
Department Chairman